X-ray diffraction, IR spectrum, optical properties, AIM, NBO, RDG, HS, Fukui function, biological and molecular docking analysis of a novel hybrid compound (C9H15N3)[CuCl4(H2O)]

Afef Gannouni, Wiem Tahri, Thierry Roisnel, Kefi Riadh

X-Ray diffraction, IR spectrum, optical properties, AIM, NBO, RDG, HS, Fukui function, biological and molecular docking analysis of a novel hybrid compound ($C_9H_{15}N_3$)[$CuCl_4(H_2O)$]

Afef Gannouni[a], Wiem Tahri[b], Thierry Roisnel[c], Kefi Riadh[a]

[a] *Laboratoire de Chimie des Matériaux, Faculté des Sciences de Bizerte, 7021 Zarzouna, Tunisie.*

[b] *Laboratory of Biochemistry and Molecular Biology, Faculty of Sciences, Risks Related to Environmental Stress, Struggle and Prevention (UR17ES20), University of Carthage, Te Ministry of Higher Education and Scientifc Research, Zarzouna, 7003 Bizerte, Tunisia.*

[c] *Université Rennes, CNRS, ISCR (Institut des Sciences Chimiques de Rennes) – UMR 6226, F–35000 Rennes, France.*

Graphical Abstract

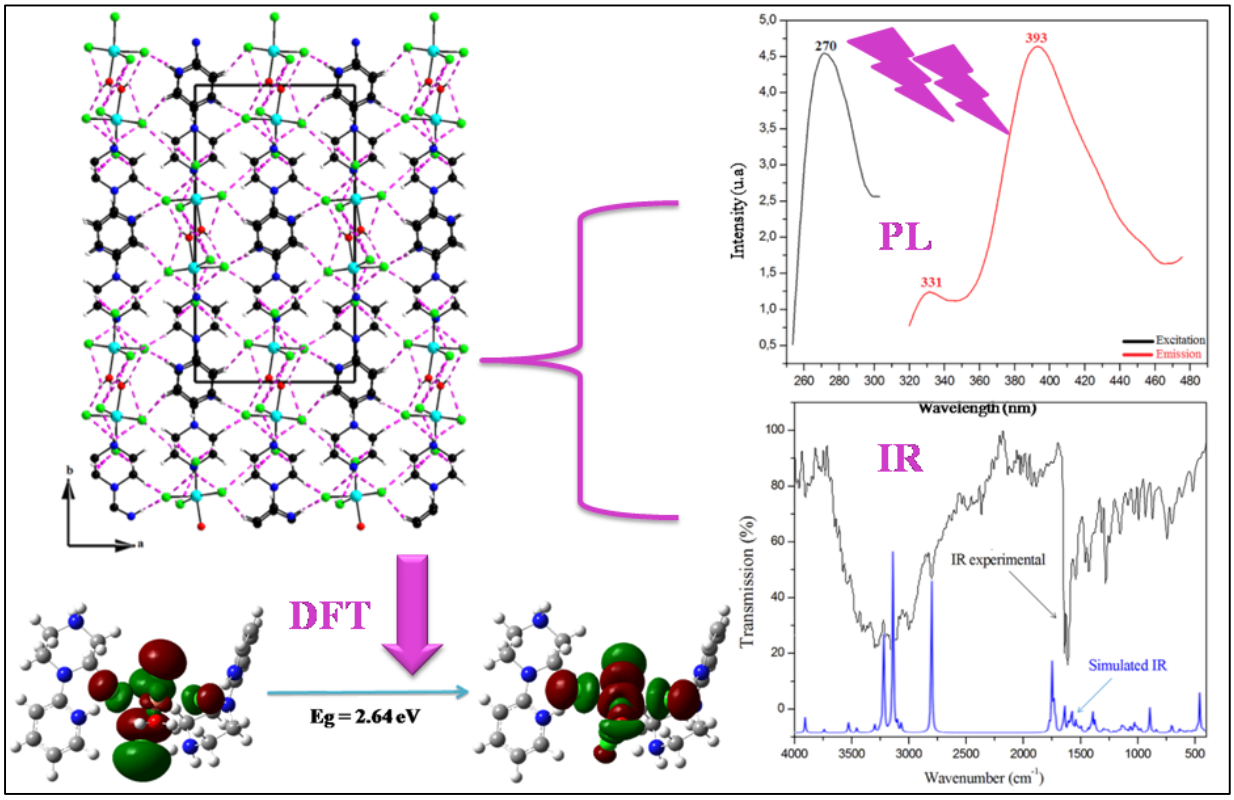

Abstract

The paper reports the preparation and structural characterization of a novel hybrid complex $(C_9H_{15}N_3)[CuCl_4(H_2O)]$ grown by slow evaporation technique in aqueous solution at room temperature and characterized by X-ray diffraction, spectroscopy measurement, optical absorption, photoluminescence proprieties, Hirshfeld surface analysis, thermal and biological study. The title organic-inorganic material, $(C_9H_{15}N_3)[CuCl_4(H_2O)]$, crystallizes in ~~the~~ monoclinic space group $P2_1/n$. The crystal arrangement consists of $[CuCl_4(H_2O)]_n^{2n-}$ chains spreading alone c axis at x= 1/2 and y= 1/2. To build the three-dimensionality of the structure, the organic cations are linked to the chains through hydrogen bond type, N – H···Cl, OW1 – H···Cl and C – H···Cl. The new prepared compound was screened for its antioxidant activity. The Photoluminescence proprieties were also reported. The nature and proportion of contacts and the rapport of enrichment in the crystal packing were studied by the Hirshfeld surfaces. The vibrational properties FT-IR and UV–VIS spectral analyses of present compound have been researched by theoretical calculations. Energy gap (Eg) of the molecule was found using LUMO and HOMO calculation. The local reactivity analyses (Fukui functions) were evaluated to identify the reactive sites in the protonated organic part. Intermolecular interactions were analyzed by molecular electrostatic potential surface (MEPS), the reduced density gradient (RDG), natural bond orbital (NBO) and topological AIM are reported. The thermal analysis (ATD/TG) reveals the decomposition of title compound. The NBO analysis of title compound shows that the maximum energy is equal to 37.61 $Kcal.mol^{-1}$ confirmed the charge transfer between organic and inorganic groups. The activation of thermodynamic parameters is calculated by DFT/ B3LYP/LanL2DZ. Photoluminescence measurements (PL) showed two peaks at around 331 and 393 nm. The biological activities of $(C_9H_{15}N_3)[CuCl_4(H_2O)]$ were investigated by DPPH and ABTS tests. Finally, docking studies have been conducted to predict 2PPCU anti-tubercular activity and as a potential therapeutic target for anticancer treatment against transaminase- Bio A and VEGFR-2 kinase inhibitor respectively type PDB's.

Keywords: *X–ray single crystal diffraction, Hirshfeld surface analysis, Fukui, RDG, AIM, biological study.*

1. Introduction

In recent years, the design and synthesis of organic-inorganic material that's on the concept of crystal engineering have attracted considerable attention regarding the application of these solids by the different proprieties of organic and inorganic components into one material.

Hybrid materials (organic-inorganic) compound represent a new class of materials when we combined desirable physical-chemical properties characteristic of both organic and inorganic components within a single molecular scale composite **[1, 2]**. In particular, the Cu^{2+} is an attractive transition metal with a d^9 electronic system and presents a variety of coordination, four **[3]**, five **[4, 5]** and six coordination **[6]** compounds predominating. The transition metal complexes, especially, Cu (II) complexes are known to be effective against rheumatoid arthritis and they also show anti-ulcer activity **[7, 8]**. The copper (II) halide complexes have played an important role in optoelectronic devices, in the developments of electronic, in optical communication and wireless temperature sensors **[9, 11]**. In addition the piperazines derivations are a family of strongly basic amines able to from dications, in which all of the N—H bonds are generally active in H-bond formation. For that, hybrid compounds with piperazines and substituted piperazines have been used in biological compounds across a number of different therapeutic areas such as antidepressant, antibacterial, antifungal, antitumor and antipsychotic **[12-13]**. The molecular docking study of hybrid compound was performed to understand the molecular interaction and binding mode **[14-16]**. In the present work, we report on our investigations on a new hybrid solid, $(C_9H_{15}N_3)[CuCl_4(H_2O)]$, how is chemical preparation and structural study are discussed, Hirshfeld surface analysis, vibrational studies, optical absorption UV-Vis and photoluminescence were performed. In addition, the theoretical studies by B3LYP were performed to analyze the structure topology using AIM, RDG, NBO and MEP analyses. The functional theory (DFT) calculations and then compared to experimental data. Finally, the molecular docking studies of the present work have been performed in the search for a therapeutic agent for the anti-tubercular activity and as a potential therapeutic target for anticancer treatment.

2. Experimental

2.1 Synthesis of $(C_9H_{15}N_3)[CuCl_4(H_2O)]$

The $(C_9H_{15}N_3)[CuCl_4(H_2O)]$ crystals were obtained by dissolving in a concentrated HCl solution a stoechiometric mixture of 1-(2-pyridyl)piperazines a solution of $CuCl_2.2H_2O$ in a minimum volume of methanol and stirring for one hour, until the formation of a clear mixture without any precipitate. The reaction mixture was stirred for half an hour resulting in a yellow-colored clear solution. The crystals can be stable for five weeks under normal conditions of temperature (yield 85%). Anal. Calc.: C: 27.79 %, N: 10.81 %, Cu: 16.35 %, Cl: 36.49 % and O: 4.11 %.

$$C_9H_{13}N_3 + CuCl_2.2H_2O + 2HCl \xrightarrow{MeOH} (C_9H_{15}N_3)[CuCl_4(H_2O)] + H_2O$$

22 X-ray single crystal structural analysis

A suitable crystal for X-ray diffraction, single crystal experiment of a new solids $(C_9H_{15}N_3)[CuCl_4(H_2O)]$ (0.510 x 0.440 x 0.190 mm^3) (***Fig S – 1***)was selected and mounted with a cryoloop on the goniometer head of a APEXII Kappa-CCD diffractometer equipped with a CCD plate detector, using Mo-K_α radiation (λ = 0.71073Å, graphite monochromator) at T = 296(2) K. Crystal structure has been described in monoclinic symmetry and $P2_1/n$ (I.T# 14) centric space group. The structure was solved by dual-space algorithm using the SHELXT program **[17]**, and then refined full-matrix least-squares methods based on F^2 (SHELXL program **[18]**). All non-Hydrogen atoms were refined with anisotropic atomic displacement parameters. Except Hydrogen atoms linked to Nitrogen atoms and of the water molecule that were introduced in the structural model through Fourier deference map analysis, H atoms were finally included in their calculated positions and treated as riding on their parent atom ~~with~~ constrained thermal parameters. A final refinement on F^2 with 3444 unique intensities and 179 parameters converged at ωR (F^2) = 0.0795 (RF = 0.0345) for 3004 observed reactions with ($I > 2\sigma$). Drawings were made with Diamond **[19]**.

2.3 Spectroscopic Measurements

The infrared spectrum was measured at room temperature in the 400–4000 cm^{-1} frequency range with a Nicolet IR200 FT-IR spectrometer. The IR spectroscopy is used to identify the functional groups and to determine the molecular structure. The UV-Vis absorption was measured at ambient temperature with a Perkin Elmer Lambda 35 UV-Vis spectrophotometer in the range of 200–1000 nm. The photoluminescence analysis was performed at room temperature by Perkin-Elmer LS55 spectrofluorometer.

2.4 Thermal analysis

The simultaneous TG-DTA analysis curves of the compound (I) were carried out in argon atmosphere at a heating rate of 5 °C.min^{-1} in the temperature range 25-700 °C on a sample of 13.1 mg.

2.5 Quantum chemical calculation

All the calculations of compound $(C_9H_{15}N_3)[CuCl_4(H_2O)]$ were carried out using Gaussian 09 W program package **[20]** with the B3LYP functional **[21, 23]** and using the LanL2DZ basis set **[24]**. The chosen cluster is built up from one $[CuCl_4\,(H_2O)]^{2-}$ triangular bipyramid and two $[C_9H_{15}N_3]^{2+}$ organic cations. All the parameters were allowed to relax and all the

calculations converged to an optimized geometry. The local minima were confirmed by the absence of an imaginary mode in vibrational analysis calculations. Theoretical vibrational spectra of the title compound were interpreted by means of potential energy distributions (PEDs) using VEDA 4 program **[25]**. For the optimized structure of the molecule in the title compound, the electronic characteristics such as HOMO and LUMO energies and the NBO analysis have a role to determine the intermolecular orbital interaction in the crystal. The iGEMDOCK program **[26]** was used, with the following parameters: population size 800, generations 80 and number of solutions 10. To represent the different docking conformations, PyMOL **[27]** was used.

2.6 In vitro Antioxidant Study

The antioxidant activity of the sample was analyzed by using DPPH an ABTS assays. The free radical scavenging ability of the title compound against DPPH (1,1-diphenyl-2 picrylhydrazyl) was evaluated as reported by Braca and al.(2001) **[28]**.Appropriate dilution of the sample (prepared at different concentrations ranging between 5 and 50 mg/ml) was mixed with 3 mL of $DPPH^{\bullet+}$ solution and incubated for 30 min in the dark. The $DPPH^{\bullet+}$ was generated by reacting a 0.1 mM DPPH (in methanol), in the dark for 40 min and adjusting the Abs at 734 nm to 0.700 with methanol. The absorbances were measured using a spectrophotometer (Shimadzu UV-Vis 160A, Japan) at 734 nm. The antioxidant activity of compound (I) was expressed as percentage inhibition of the $DPPH^{\bullet+}$ radical which was subsequently calculated by using the following equation:

$DPPH^{\bullet+}$ radicals scavenged activity (%) = [(A0 − A1)/A0] × 100. where A0 and A1 refer to the absorbance measured for the reaction mixture without and in the presence of the test of $(C_9H_{15}N_3)[CuCl_4(H_2O)]$ compound, respectively. The $ABTS^{\bullet+}$ scavenging ability of title compound were determined according to the method described by Guesmi and al. (2014) **[29]**. The $ABTS^{\bullet+}$ was generated by reacting an (7 mmol/L) ABTS aqueous solution with sodium acetate buffer (20 mM, pH 4.5) in the dark for 16 h (4 °C) and adjusting the Abs at 734 nm to 0.700 with ethanol. A measurement of 20 µL of sample (I) at different concentrations was added to 3 mL $ABTS^{\bullet+}$ solution and reaction mixture was allowed to stand at 30 °C the absorbance were measured using a spectrophotometer (Shimadzu UV-Vis 160A, Japan) at 734 nm after 30 min. The percent scavenging of $ABTS^{\bullet+}$ was calculated using the formula: **$ABTS^{\bullet+}$ radicals scavenged activity (%) = [(A0 − A1)/A0] × 100**. where A0 and A1 refer to the absorbance measured for the reaction mixture without and in the presence of the tested compound, respectively.

3. Results and discussion

3.1 Structure description

The 1-(2-pyridinium) piperazinium aquatetrachloridocuprate (II) (Abbreviated 2PPCU) crystallizes in monoclinic space group $P2_1/n$ (Z= 4), with a= 10.2986 (8) Å, b= 19.1385 (13) Å, c= 7.6984 (5) Å, β= 90.134(4)° at T=173K, as deduced from X-ray single crystal diffraction study. A summary of the crystallographic data and the structure refinement results is given in **Table 1**. Configurations of the different organic and inorganic species, including the vibrational ellipsoids at 50% probability are depicted in **(Fig. 1)**. The Cu (II) atom is four-fold coordinated by chloride ions and one molecule H_2O, forming a triangular bipyramid. The atomic arrangement of $(C_9H_{15}N_3)[CuCl_4(H_2O)]$ can be described as built up by inorganic chains of $[CuCl_4(H_2O)]^{2n-}$ triangular-based bipyramid extending along the c direction held together by O – H···Cl hydrogen bonds **(Fig. 2**, **Table 2**). Four such chains cross the unit cell at x = ½ and y = ½ **(Fig. 2)**. The organic groups are located between these chains and connect to them through N – H···Cl and C – H···Cl hydrogen bonds to form a three dimensional infinite network. In addition, the N – Cl and H (N)···Cl distances varying between 3.093-3.386 Å and 2.71-2.34Å, respectively. While, the OW1 – Cl and H (OW1)···Cl distances are between 3.179 - 3.231Å and 2.36-2.43Å, respectively. Furthermore, the N – H···Cl, OW – H···Cl and C – H···Cl angles are varying between 133-157°, 150.6-151.4° and 129.3-156.6°, respectively. The description of $[CuCl_4(H_2O)]^{2-}$ entity is justified by Cu1 – Cl bond length from 2.2650 (8) to 2.5494 (9) Å and Cu1 – O bond distances which equals 1.996 (2) Å. Meanwhile, the Cl – Cu1 – Cl bond angles range between 93.51(3) and 160.49(4)° and O – Cu1 – Cl bond angles vary from 84.22(8) to 168.40(9)° **(Table 3)**. In addition, the calculated average values of the distortion indices as described by Baur **[30]** corresponding to the different distances and angles in $[CuCl_4(H_2O)]$, ID (Cu1 – Cl (O)) = 0.2288 and ID (Cl – Cu1 – Cl(O)) = 22.753, show a remarkable distortion due to the existence of two types of ligands (Cl and O) of different electronegativities surrounded by copper and the different electrostatic interactions between these entities.

The asymmetric unit contains a single organic entity 1-(2-pyridinium) piperazinium. C–C distances values are between 1.344 (5) and 1.502 (2) Å, N–C distances are between 1.338 (4) and 1.497(4) Å, C–C–C angles are from 118.2(3)° to 121.2(3)°, N–C–C angles are between 108.9(3)° and 125.0 (3)° and C–N–C angles range from 111.4(2)° to 124.5(3)°. The main geometrical characteristics of these entities are grouped in **(Table 4)**. Examination of the organic cation shows that the piperazine fragment is cyclic, it adopts the most stable chair

conformation characterized by the following Puckering parameters: q_1 = 0.5681 Å, q_2 = 0.0273 Å, q_3 = 0.5764, θ = 2.75° and φ = 15.74° **[31]**.

3.2 Hirshfeld surface

In order to analyze the function of the organic base in structural propagation, Hirshfeld surface analyses on $(C_9H_{15}N_3)[CuCl_4(H_2O)]$ were carried out. Hirshfeld surface has been calculated using Crystal Explorer 3.1 **[32]**. The contributions from different interaction types of title compound which overlap in the full fingerprint is represented in the **fig. 4**a. The 3D d_{norm} surfaces representation of the Hirshfeld surface makes it possible to identify the contacts that take place between the organic $[C_9H_{15}N_3]^{2+}$ and inorganic $[CuCl_4(OH_2)]^{2-}$ entities previously studied **(Fig. 4**b**)**. The Hirshfeld surface of the asymmetric unit mapped with d_{norm} property, the large circular depressions (deep red) are indicators of hydrogen bonding contacts, which can be attributed to interactions of the N – H···Cl, OW – H···Cl and C – H···Cl interactions. The shape index **(Fig. 4**c**)** and the curvedness **(fig. 4**d**)** are the most suitable for identifying the π – π interactions. In present compound, the curvedness map represents the large flat green areas delimited by bold blue outline around the pyridinium cycle; moreover the shape index has the adjacent red and blue triangles which confirm the presence of the π – π stacking interactions between two neighboring pyridinium rings.

The 2D fingerprint plots were displayed by using the standard view with the d_e and d_i distance scales displayed on the graph axes obtained by Hirshfeld surface analysis. Globally, H···Cl/Cl···H, and H···H interactions were most abundant in the crystal packing (54.1, 31.5 % respectively) **(Fig S–2)**. On the cation $[C_9H_{15}N_3]^{2+}$ and anion $[CuCl_4(H_2O)]^{2-}$ in the asymmetric unit, these contacts are attributed to hydrogen bonds, N – H···Cl, OW1 – H···Cl and C – H···Cl. Therefore, the Cl···H contacts represent the hydrogen bonds which have more than half of the total Hirshfeld area (54.1%) and have a slightly enriched E = 1.57. The Cl···H contacts appear two sharp symmetric spikes in the 2D fingerprint maps with a prominent long spike at de + di = 2.2 Å. The fingerprint plots of different Hirshfeld surfaces were decomposed into fractions due to individual atom types to highlight particular atom pair close contacts. This analysis shows that for $[C_9H_{15}N_3]^{+2}$, the complementary regions result from two types of close contacts: C···C (4.2%) and N···C (1.5%). These interactions have fairly high enrichment values of E_{CC} (36.99) and E_{NC} (8.33), indicates the presence of π – π interactions. Red hollows on the second side result from interactions C (π)···Cl (0.4%) have a high enrichment ratio E = 2.22. Moreover, the O – H interactions represent 1.8% to the total Hirshfeld surfaces and appear as two shap spikes in the two-dimensional fingerprint maps with de + di = 2.8 Å. These interactions have fairly high enrichment values of E_{OH} = 1.5

attributed to hydrogen bonds types (OW – H···Cl). The N – H and Cl – O contact in fingerprint plots (1.6% and 0.1%, respectively) have enrichment ratios of 0.82 and 0.19, respectively. The Cl···H is the driving forces in the molecular arrangement **(Table 5)**. Finally, the Hirshfeld surface and related fingerprint plots of $(C_9H_{15}N_3)[CuCl_4(H_2O)]$ complex have been presented in order to understand the nature of intermolecular interactions and stability of the molecule.

3.2 Vibrational analysis

To give more information on the structure 2PPCU we have studied the vibration proprieties of the title compound, using infrared absorption spectroscopy at room temperature, to better assign the vibration modes we use the theoretical calculations (DFT). The experimental (b) and theoretical (a) infrared spectra are shown in **Fig. 5**. Furthermore, in **Table S – 1**, we have gathered assignment attempts of IR vibrational modes based mainly on the theoretical results. The IR spectrum is clearly composed of five absorption bands in the 3642 – 2800 cm^{-1} range, which is assigned to the symmetric and asymmetric valence vibration modes ν(OH), ν(NH_2), ν(CH), ν(NH) and ν(CH_2). The theoretical calculation of this compound made in gaseous phase (free hydrogen bond) for this reason, the vibration bands are delimited (between 3695 and 3007 cm^{-1}). Moreover, the peaks located at 1627, 1531, 1450 and 1607 cm^{-1} can be attributed respectively to the deformation vibrations (NH_2), (NH) and (CNC), to the valence vibration of (C = C). In addition, the peak detected at 1547 cm^{-1} corresponds to the deformation vibration of the water δ (H_2O). The valence and deformation vibrations of (C – C) are between 1414-900 cm^{-1} and 1515-1220 cm^{-1} respectively. The vibrations between 1520 and 1500 cm^{-1} correspond to the symmetric and asymmetric deformation of the CH. The vibration bands in the range 1450-1200cm^{-1} are assigned to valence and deformation (CN) vibrations. The peak around 1220cm^{-1} corresponds to δ_{as} (CC). The vibrations between 1100 and 723cm^{-1} correspond to the symmetric and asymmetric deformation of (NCC) and (CCC). The group of peaks at 1438-890 cm^{-1} can be attributed to the modes of movement, torsion (HNCC), (HCNC), (HCCN), (CCNC) and (HCCC). Finally, the peak around 650 cm^{-1} confirms the out-of-plane vibrations of the links (CCCN). It is worthily noting the relative good agreement observed between the theoretical and experimental vibrational modes. This is well proved with the best correlation between almost all the observed and calculated vibrational frequencies depicted in the correlation graph shown in **Fig S – 3** (The calculated correlation coefficient (R) is 0.99903).

3.4 Optical study

The experimental and the theoretical UV-Visible absorption spectrum of $(C_9H_{15}N_3)[CuCl_4(H_2O)]$ are gathered in **(Fig S – 4)**. The title solid exhibits a wide optical absorption between 200 and 1000 nm at room temperature. The results reveal that the present compound have four bands at λ = 281.25 nm, λ = 295.80, λ = 323.39 and at λ = 463.16 nm attributed to TCML, $\pi \rightarrow \pi^*$ and $n \rightarrow \pi^*$ transitions, TCML and TC anions–cation, respectively **(Table 6)**. The strong absorption at 350 nm is relative to the aromatic conjugation in the cations $(C_9H_{15}N_3)^{2+}$. The Kubelka-Munk theory (K.M) is generally used for analyzing the diffuse reflectance spectra obtained from weakly absorbing compounds. The Kubelka-Munk remission function is given by the following form **[33]**: F(R) = (1-R)/2R, where R is the reflectance of $(C_9H_{15}N_3)[CuCl_4(H_2O)]$ and F(R) is the Kubelka-Munk function. **Fig S – 5 (a)** and **(b)** present the plots of the diffuse reflectance spectrum and the (K.M) curve of present compound, respectively at different wavelengths. Assuming a direct band gap energy of the title compound [$\mathbf{(F(R) \times h\nu)^2 = h\nu}$], the extrapolation of the linear part of the TAUC plot method extraction **[34]** indicates a band gap energy Eg = 2.05 eV in **Fig. 6**. This result was similar to compound $(C_7H_7N_2S)[CuCl_4]$ **[35]**. The absorption peaks found in the absorption spectrum are very similar to those observed in other previously reported organic–inorganic compound.

The frontier molecular orbitals are two types: highest occupied molecular orbital (HOMO) and lowest unoccupied molecular orbital (LUMO). The difference between these two orbitals called gap energy is useful to characterize the chemical stability of a molecule. A high gap indicates a high stability of the molecule and therefore low reactivity and vice versa. The HOMO, HOMO-1, LUMO, LUMO+1 orbitals as well as the gap energy, calculated in the gas phase are mapped in **Fig. 7** in which red and green regions represent positive and negative phase, respectively. The energy values of HOMO, LUMO, LUMO+1, HOMO-1 were calculated from the TD-DFT method associate B3LYP/LanL2DZ is: E_{HOMO} = -10.909 eV; E_{LUMO} = - 8.27 eV; E_{LUMO+1} = - 6.922944 eV; E_{HOMO-1} = - 11.133232 eV, corresponding to HOMO-LUMO gap of 2.64 eV. This value was similar to compound $\{(C_{12}H_{22}N_2)[CuCl_4]\}$ **[36]**. Moreover the E_{HOMO} and E_{LUMO} values are easily used to calculate the chemical hardness (η = (I-A)/2), the global softness (S = 1/2η), the electron affinity (I = -E_{HOMO}) and the ionization potential (A = -E_{LUMO}). Also, the values of electronegativity can be determined according to the definition of Mulliken **[37]** (χ = (I+A)/2), the global chemical potential (μ = - (I+A)/2) and the global electrophilicity introduced by Parr et al. **[38]** ($\omega = \mu^2/2\eta$).The chemical softness (S) and Hardness (η), of the molecule study, are related to gap energy. If the crystal has small gap energy makes the molecule as soft. These molecules are

more polarizable because they need a small energy for excitation. The potential μ (-9.5895) is negative which means that the title compound is stable. **Table 7** regroups all the calculated values of chemical reactivity descriptors. The optical transmittance spectrum of $(C_9H_{15}N_3)[CuCl_4(H_2O)]$ is obtained from the absorption spectrum **(Fig S – 6)**. For any material the optical transmission range, transparency cut-off and the absorbance band are the most important optical parameters for laser frequency conversion applications. In our hybrid compound the transmission percentage does not exceed 27% transmission in the visible region and cut-off wavelength was found to be λ = 300 nm. The absence of absorption in the visible region (300-900 nm) reveals that our crystal $(C_9H_{15}N_3)[CuCl_4\ (H_2O)]$ could be exploited for optical applications.

3.5 Photoluminescence properties

The emission spectrum of $(C_9H_{15}N_3)[CuCl_4\ (H_2O)]$ at room temperature is shown in **Fig S – 7**. The excitation of compound (I) with λ_{ex} = 270 nm reveals that luminescence band is located at two positions. The fluorescence spectrum shows two peaks in increasing order of intensity, 331 and 339 nm, respectively. The emission band located at λ_{em1} = 331 nm is probably due to $\pi^* \rightarrow \pi$ and $\pi^* \rightarrow$ n transition of 1-(2-pyridinium)piperazinim. The emission band observed at λ_{em2} = 339 nm can be attributed to ligand-metal charge transfer (LMCT) transition.

3.6 NBO analysis

The NBO analysis of $(C_9H_{15}N_3)[CuCl_4(H_2O)]$ structure presents the high electro-negativity of chlorine; oxygen and nitrogen give a high value of polarization coefficients **(Table S – 2)**. The second order perturbation theory analysis of the Fock matrix in natural bond orbital (NBO) basis shows strong intermolecular hyper conjugative interactions. These interactions are formed by orbital which results in an intermolecular charge transfer causing stabilization of the system. In **table S – 3** the perturbation energies of donor-acceptor interaction are presented. In our title molecule $(C_9H_{15}N_3)[CuCl_4(H_2O)]$, the LP(Cl4) – LP*(Cu1) has 37.61 Kcal.mol^{-1}, LP(Cl5) – LP*(Cu1) has 28.63 Kcal.mol^{-1}, LP(Cl3) – LP*(Cu1) has 26.26 and LP(Cl2) – LP*(Cu1) has 15.54 Kcal.mol^{-1}, these energies confirmed the charge transfer between organic and inorganic entities. The interaction LP(O6) – LP*(Cu) have the stabilization energy equal 26.15 Kcal.mol^{-1}. In addition, the LP(N20) – π*(N17 – C19) having the stabilization energy 22.94 Kcal.mol^{-1} are responsible for hyper conjugation in organic entities. Furthermore, the interactions π (N17 – C19) – π*(C9 – C11) and π*(C13 – C15) having the stabilization energy 23.72 Kcal.mol^{-1} and 11.66 Kcal.mol^{-1}, respectively. The interaction π (C9 – C11) – π*(N17 – C19) and π* (C13 – C15) having the stabilization energy

21.48 Kcal.mol^{-1}and 6.97 Kcal.mol^{-1}, respectively. The π (C13 – C15) – π*(N17 – C19) interactions having an E (2) = 6.71 Kcal.mol^{-1}. These important interactions prove the existence of ππ interaction in our compound. Finally, the LP(Cl3) – σ* (N17 – H18) interactions having the stabilization energy 8.53 Kcal.mol^{-1}, which shows the presence of intermolecular N–H···Cl hydrogen bond in title compound. Finally, to investigate the chemical reactivity and stability of the title complex, we carried out the quantum descriptors analysis, the natural bond orbital (NBO) helps us to study the intra and intermolecular interactions.

3.7 Molecular electrostatic potential surface (MEPS)

The molecular electrostatic potential of $(C_9H_{15}N_3)[CuCl_4(H_2O)]$ was calculated by B3LYP/6-31 G*. The maximum positive region, which preferred site for nucleophilic attack symptoms as blue color and the maximum negative region, which preferred site for electrophilic attack indicate as red color. The importance of MEP lies in the fact that is simultaneously display molecular size, shape as well as negative, neutral and positive electrostatic potential regions. MEPS analysis allows the determination of electron-donor and electron-acceptor sites, which is especially useful for investigation the intra and intermolecular interactions such as hydrogen bonding. In title compound, the negative electrostatic potential sites are on the chlorine atoms surrounding the Cu atoms, whereas the positive electrostatic potential sites are on the hydrogen of the nitrogen atoms in $[C_9H_{15}N_3]^{2+}$ cation **(Fig S – 8)**. The dispersion of potential in the title compound is -4.191 a.u to 0.290 a.u. Finally, the molecular electrostatic potential confirms the X-Ray results in the existence of an N-H…Cl intermolecular interaction.

3.8 Reduced Density Gradient (RDG) analysis

The weak interactions play an important role in many chemical, physical, or biological phenomena **[39]**. They can be used in various applications such as hydrogen storage for renewable energies **[40]**. Reduced density gradient (RDG) is a very popular and powerful method for analyzing weak interactions such as repulsive interactions, Van der Waals interactions and hydrogen bonds using a simple color code. The RDG approach is based on the charge density introduced by Johnson and al. **[41]** and Contreras-Garcia and al. **[42]**. **Fig S – 9 (a)** and **(b)** gives a visualization of non covalent interaction in the molecular space of 2PPCU molecules by using VMD and Multiwfn programs **[43, 44]**, respectively. **Fig S – 9 (b)** illustrates the RDG function versus the electron density ρ multiplied by the sign of the second eigenvalue $\lambda 2$ for $(C_9H_{15}N_3)[CuCl_4(H_2O)]$ compound. Through a color code we can differentiate between different regions of interactions (show **Fig S – 9 (c)**). This figure

highlights regions of color that allow us to describe the type of interaction. When sign ($\lambda 2)\rho$ takes a negative value, we have a strong attractive interactions (blue color). The last case, we have Van der Waals interactions when sign ($\lambda 2)\rho$ is close to zero (green color). Strong repulsive interactions when sign ($\lambda 2)\rho$ has a positive value (red color). As clearly seen, the blue spot between the hydrogen atom carried by the nitrogen atom and the chloride atom indicates the formation of a strong attractive interaction N – H···Cl. Moreover the green plates with slight brown located between the anionic and cationic entities, are attributed to Van der Waals interactions and the elliptic red plate located in inorganic part $[CuCl_4]^{2-}$ is related to repulsive interactions. Along with this, the non-covalent interaction shows that strong repulsive interactions showed from two spikes along with sign ($\lambda 2$) positive values, located at the center of the cycle are related to repulsive interactions present between the atoms of aromatic molecules.

3.9 Quantum theory of atoms in molecules (QTAIMs) analysis

Atoms-In-Molecule (AIM) analysis is an efficient tool to determine the presence of critical points (CPs) of $(C_9H_{15}N_3)[CuCl_4\,(H_2O)]$. This point is used for the identification of chemical bonds between atoms and interatomic interactions. The topological parameters proposed by Bader **[45]** can be calculated in the bond critical point using the Multiwfn program [44] such as the electron density ρ(r), the Laplacien values $\nabla^2\rho(r)$, the elliplicity (ε), which makes it possible to evaluate the properties of the bonds in the compound and more particularity the hydrogen bonds. The latter can be classified into three categories according to Rozas and all [46]. A strong or very strong hydrogen bonds: $\nabla^2\rho$ (rBCP) < 0 and H (rBCP) < 0, a moderate hydrogen bonds: $\nabla^2\rho$ (rBCP) > 0 and H (rBCP) < 0 and a weak hydrogen bonds: $\nabla^2\rho$ (rBCP) > 0 and H (rBCP) > 0.

The graphical representation of AIM analysis of title compound is illustrated in **Fig. 8** and the calculated topological parameters are assembled in **Table 8**. The AIM topological analysis reveals that our crystal is stabilized by six hydrogen bonds H···Cl. The BCP analysis in **Table 8** shows that the six hydrogen bonds H···Cl are considered a moderate hydrogen bonds energies of -69.5697, -88.8643, -107.6828, -91.6268, -77.3533 and -90.5268 $Kcal.mol^{-1}$, and the energy density (0.2061250, 0.2641818, 0.3208060, 0.2724941, 0.2295457 and 0.2691843 a.u) confirm the strength of these hydrogen bonds compared to other compounds **[47]**. These values are greater than zero according to the Rozas criterion. In addition, the AIM analysis allows us to detect the presence of cycles in a molecular system through the presence of a new ring critical point RCP1, RCP2, NRCP1, NRCP2 and NRCP3 cycles that are formed through the interactions between the organic group and the inorganic anion via hydrogen bonds.

Finally, the study of atom-atom interactions in the present compound was explored with the aid of the quantum theory of atom-in-molecule (QTAIM) to confirm la presence of H…Cl hydrogen bonds.

3.10 Fukui function

Fukui function is recognized as highly a recommendable local reactive factor. Fukui functions are prominent functions which give idea related to the capacity of the molecule to accept or donate an electron. Therefore, reveal information about an atom being nucleophilic or electrophilic. Generally, nucleophilic f^+ (r) and electrophilic f^- (r) attacks are computed via Fukui function. f^- = N – (N - 1) and f^+ = (N + 1) – N; the atomic charge of cationic $(C_9H_{15}N_3)^{2+}$, anionic $(C_9H_{15}N_3)$ and neutral $(C_9H_{15}N_3)^+$ calculated by B3LYP/6-311++G (p, d) level of theory. Besides, to get Fukui's functions, the neutral molecule is calculated to know the corresponding molecular structure two of the lowest energy and its multiplicity. The molecular geometry obtained above makes it possible to calculate on its anion and its cation while changing the charge and the multiplicity in each case. Therefore, more than MEPS that allows recognizing nucleophilic and electrophilic sites; these sites can be identified from these Fukui's functions. From **Table S – 4**, it is observed that the higher Fukui function f^+ values are in order of 18C> 2C> 5C> 3C> 15C> 12C> 11N> … etc, these are the nucleophilic attack sites. In addition, higher Fukui function f^- values are in order of 4C> 19H> 12C> 24N> 15C> 17H> 25H> 23H> 6H> 7H> 9H> … etc, these are the electrophilic attack sites. Dual descriptor f (r) exposes a reactive site more suitably **[48]**. It is presented by, $\Delta f = f^+ - f^-$. The Δf provides an effective distinction among nucleophilic and electrophilic attack at accurate region along their sign.

- If $\Delta f < 0$, the site is favorite for electrophilic attack.
- If $\Delta f > 0$, the site is favorite for nucleophilic attack.

For that, we have shown in **Fig. 9**, the variation of Δf in functions of the atoms. Results reveal that, from the calculated values of Δf given in **Table S – 4**, the atoms 1C, 2H, 4C, 6H, 7H, 8H, 9H, 10N, , 14H, 15C, 16H, 17H, 20H, 21C, 23H, 24N and 25H present electrophilic sites since the value of Δf is negative. It is seen that the atoms 1C (Δf = -1.939) are the favorable sites for electrophilic attack. While, 2C, 3C, 5C, 11N, 12C, 13H, 18C and 19H correspond to the positive Δf so they present the nucleophilic sites. 18C and 2C are the favorable sites for nucleophilic attack where Δf equal to 2.109 and 1.629, respectively.

Fig. 9 mentioned the Fukui functions (f^-, f^+ and Δf) of $(C_9H_{15}N_3)^{2+}$ are shown. The Fukui Function (FF) confirms the protonation to be done on N10 or N11. When the amine

protonated only once, the second protonation was made on N10, Fukui's calculation confirms the experimental results since N10 is more favorable by electrophilic attack than N11.

3.11 Thermal study

The differential thermal and thermogravimetric analysis (ATD/ATG) of the title compound produced by a mass of 13.1 mg, a temperature varies between 25-700 °C with a heating rate equal to 5 °C.min^{-1} and under an atmosphere of argon are given in **Fig S – 10**. Our compound $(C_9H_{15}N_3)[CuCl_4(H_2O)]$, loses its water molecule at 150 °C, the loss of mass is Δm1= 4.616%, corresponds well to the loss of relative theoretical mass at the start of the coordinating water molecule of the compound (theoretical mass loss ≈ 4.6%). The endothermic peak located at 210 °C can be assigned to the release of two molecules of hydrochloric acid, good agreement with the experimental mass loss (Δm2 ≈ 10%) and the calculated mass loss (9.4 %). The $(C_9H_{15}N_3)[CuCl_4(H_2O)]$ compound is stable at temperatures below 373 K.

3.12 Biological study

In vitro antioxidant activity of 2PPCU showed an interesting scavenging activity in both the DPPH and ABTS tests. The antioxidant capacities of title compound are summarized in **Fig S – 11**. The highest antioxidant capacities were detected for title compound by DPPH assay (a percentage of inhibition 57.95% ±7.05 at 50 mg.ml^{-1}).This finding was confirmed by the result obtained in the ABTS test (51.20% ± 0.55 at 50 mg.ml^{-1}). This in vitro scavenging activity can be explained by the proton diffusion ability as well as the composition of $(C_9H_{15}N_3)[CuCl_4(H_2O)]$ which contains reactive sites such as Nitrogen, Chlorine and Carbon atoms, which could be proton donors or electron acceptors.

3.13 Molecular docking

In order to explore the different modes of binding that can be established between 2PPCU as a new protein inhibitor candidate, we have chosen eight co-crystal structures removed from the protein data bank (pdb) with the following codes: 4MQQ, 6GQO, 6GQP, 3TFT, 3G60, 3PWH, 3W37 and 1Y6B. All ligands and water molecules are removed for each protein and hydrogen atoms are added to them using Autodock Tools **[49]**. **Table 8** summarizes the docking energies with the different proteins. We have carried out this work with 5 poses for each protein and we have represented only the best poses which represent the minimum energy. This minimum is the sum of three types of interaction, namely VDW, H-band and electronic binding energy. According to the results found in **Table 9**, it is clear that the two proteins 4MQQ and 6GQO show strong interactions with energies respectively equal to -96.5416 and -96.4865 Kcal.mol^{-1}. Moreover, the proteins receptors 4MQQ have strong

interactions in similar bibliographic **[50]**. We can see that the compound 2PPCU makes electronic interactions with all the proteins except for 3G60 and 1Y6B. H-Bond-like interactions with the 6GQO protein are most intense, while the strongest VDW-like interactions are with the 4MQQ protein. **Fig S – 12** illustrates the intermolecular interaction between the 2PPCU ligand and the proteins 4MQQ, 6GQO, while **Fig S – 13** shows those established with 6GQP, 3TFT, 3G60, 3PWH, 3W37 and 1Y6B. The analysis of **Fig. 10 – a** (protein 6GQO) shows three polarized interactions. Two with residue ARG-1126 type N – H···N and one with ARG-1118 type N – H···Ow. On the other hand, for **Fig. 10 – b** (protein 4MQQ), the inorganic group $[CuCl_4(H_2O)]$ plays the role of an electron acceptor residue TYR-25 via its alcohol function. Finally, the activity of 2PPCU compound against transaminase-Bio A type PDB (4MQQ) and with VEGFR-2 kinase inhibitor with respect to one of these receivers (6GQO), which reveals respectively the anti-tubercular activity and as a potential therapeutic target for anticancer treatment. These results have a good agreement with similar article **[51]**.

Conclusion

Finally, the present compound $(C_9H_{15}N_3)[CuCl_4(H_2O)]$, was prepared as single crystals at room temperature and characterized by physicochemical methods. On the structural level, the atomic arrangement of this material consists of a network of $[CuCl_4(H_2O)]^{2-}$ anions and 1-(2-pyridinium) piperazinium cations $[C_9H_{15}N_3]^{2+}$ connected by OW1 – H···Cl, N – H···Cl and C – H···Cl hydrogen bonding interactions. Investigation of intermolecular interactions and crystal packing via Hirshfeld surface analysis reveals that the structure is maintained primarily by H···Cl strong hydrogen bonds and hydrophobic contacts H···H. The shape index and curvedness represents a π – π stacking interactions between two neighboring pyridinium rings. In fact, the vibrational spectrum (FT-IR) and the UV-Visible absorption calculated by DFT are in good agreement with the experimental results. Furthermore, the HOMO-LUMO energy gap value (Eg = 2.64 eV) confirmed that this compound can be classified as semiconductor material. The optical properties of title compound were investigated by UV–Vis absorption and photoluminescence measurements and revealed that the complex exhibits a blue light emission at room temperature. The NBO analysis indicated that the N–H···Cl, C–H···Cl, $\pi \rightarrow \pi^*$ and $n \rightarrow \pi^*$ intermolecular interactions significantly influence crystal packing in $(C_9H_{15}N_3)[CuCl_4(H_2O)]$. This result has been confirmed by Hirshfeld surface analysis. Moreover, the AIM and RDG approach suggests a good stability of the title compound. MEPs

mapping and Fukui function are determined to predict the electrophilic and nucleophilic reactions also the hydrogen bonding interactions of the molecule. Fukui's calculation confirms the experimental results since N10 is more favorable by electrophilic attack than N11. Finally the bioassay results showed that the structure exhibits significant antibacterial activity and the activity of 2PPCU molecule against proteins receptor 4MQQ and 6GQO is significant with a binding energy of -96.5416 and -96.4865 Kcal.mol^{-1} respectively.

Acknowledgments: We are grateful to the Tunisian Ministry of Higher Education Scientific Research for the provided financial support

Supplementary Data: CCDC 2069472 contains all data related to this crystal.

Conflict of interest: The authors don't have any conflict of interest.

Highlights

*A New Organic-Inorganic Hybrid Compound $(C_9H_{15}N_3)[CuCl_4(H_2O)]$ was successfully synthesized and structurally characterized.

*Intermolecular interactions were explored using Hirshfeld surface analysis and RDG approach.

*Optical properties and vibrational bands of the compound were discussed and investigated by DFT calculations.

*Antibacterial activity of compound has been tested by DPPH and ABTS.

*Molecular docking studies confirmed the inhibitory activity of $(C_9H_{15}N_3)[CuCl_4(H_2O)]$.

References

[1] C. R. Mariappan, G. Govindaraj, S. Vinoth. Rathan, G. Vijaya. Prakash, Mater. Sci. Eng. B 123 (2005) 63-68.

[2] David. B. Mitzi. Phillip Brock. Inorg. Chem. 40 (2001) 2096-2104.

[3] A. Hachani, I. Dridi, A. Othmani, T. Roisnel, S. Humbel, R. Kefi, J. Mol. Struct. 1229(5) (2020) 129838.

[4] A. Kessentini, M. Belhouchet, J. J. Sunol, Y. Abid, T. Mhiri. Spectrochim. Acta A. Mol. Biomol. Spectrosc. 134 (2015) 28.

[5] P. Arularasan, B. Sivakumar, G. Chakkaravarthi, R. Mohana, Acta Cryst. E 69, (2013), 583.

[6] T. Dammak, H. Boughzala, A. Mlayah, Y. Abid, J. Lumin. 173 (2016) 213.

[7] R. H. Al-Far R H, B. F. Ali, J. Chem. Crystallogr, 38 **(**2008) 373.

[8] Sorenson J R J 1976 J. Med. Chem, 19 135

[9] A. Kessentini, M. Belhouchet, J. J. Sunol, Y. Abid, T. Mhiri, J. Luminescence. 149 (2014) 341-347.

[10] R. Almairac, A. Astito, J. Lapasset, J. Moret, P.Saint-gregoire, J. Ferroelectr. 125 (1992) 203-208.

[11] N. Drissi, K. Karoui, F. Jomni, A. Ben Rhaiem, Phys. E Low Dimens. Syst. Nanostructures. 83 (2016) 349-357.

[12] Humle, C. Cherrier, M.P.Tetrahedronlett, 40 (1999) 5295-5299.

[13] S. Bhati, V. Kumar, S. Singh, J. Singh, Synthesis, biological activities and docking studies of piperazine incorporated 1, 3, 4-oxadiazole derivatives, Journal of Molecular Structure. 1191 (2019) 197-205.

[14] O. Noureddine, S. Gatfaoui, Silvia Antonia Brandán, H. Marouani, N. Issaoui, Structural, docking and spectroscopic studies of a new piperazine derivative, 1-Phenylpiperazine-1,4-diium bis (hydrogen sulfate), Journal of Molecular Structure. 1202 (2020) 127351.

[15] Alaa Z.Omar, Tawfik M.Mosa, Samer K.El-sadany, Ezzat A.Hamed, Mohamed El-atawy, Novel piperazine based compounds as potential inhibitors for SARS-CoV-2 Protease Enzyme: Synthesis and molecular docking study, Journal of Molecular Structure. 1245 **(**2021**)** 131020**.**

[16] H. S. Nagendra Prasad, A. P. Ananda, T. N. Lohith, P. Prabhuprasad, H. S. Jayanth, N.B. Krishnamurthy, M. A. Sridhar, L. Mallesha, P. Mallu, Design, synthesis, molecular docking and DFT computational insight on the structure of Piperazine sulfynol derivatives as a new

antibacterial contender against superbugs MRSA, Journal of Molecular Structure. 1247 **(**2022**)** 131333**.**

[17] G. M. Sheldrick. Acta. Cryst. (2015) A71 3-8.

[18] G.M. Sheldrick. Acta. Cryst. (2015) C71 3-8.

[19] K. Brandenburg, Diamond Version 2.0 Impact GbR. Bonn, Germany, (1998).

[20] M.J. Frisch, G.W. Trucks, H.B. Schlegel, G.E. Scuseria, M.A. Robb, J.R. Cheeseman, G. GAUSSIAN 09, Revision A.1, GAUSSIAN, Inc, Wallingford CT, 2009.

[21] A.D. Becke, Phys. Rev. 38 (1988) 3098–3100.

[22] A.D. Becke, J. Chem. Phys. 98 (1993) 1372–1377.

[23] C. Lee, W. Yang, R.G. Parr, Phys. Rev. B 37 (1988) 785–789.

[24] P.J. Hay, W.R. Wadt, J. Chem. Phys. 82 (1985) 270–283.

[25] M.H. Jamroz. Vibrational Energy Distribution Analysis: VEDA 4 Program, Warsaw, Poland (2004). http://www.smmg.pl.

[26] J.M. Yang, C.C. Chen, GEMDOCK: A Generic Evolutionary Method for Molecular Docking, Proteins Struct, Funct, Bioinf, 55 (2004) 288–304.

[27] W.L. DeLano, PyMOL DeLanoScientific, 700, San Carlos, CA, 2002

[28] A. Braca, N. De Tommasi, L. Di Bari, C. Pizza, M. Politi, I. Morelli, Journal of Natural Products, 64 (2001) 892-895.

[29] G. Fatma, Ben Farhat Mouna, M. Mejri, A. Landoulsi, Lipids in Health and Disease, 13 (2014)114.

[30] W. Baur, Acta Cryst, (B30), 1974, 1191-1195

[31] D. Cremer and J. A. Pople (1975). J. Am. Chem. Soc. 97, 1354–1358.

[32] J.J. McKinnon, M.A. Spackman, A.S. Mitchell, Acta. Crystallogr. B B60 (2004) 627–666.

[33] Y. Dang, L. Yang, S. Youxuan, Y. Dongsheng, L. Xiaolong, L. Weiqun, L. Guangfeng, X. Haibing, T. Xutang, J. Cryst. Eng. Comm. 17 (2015) 665–670.

[34] J. Tauc, J. Mater. res. Bull. 3 (1968) 37–46.

[35] A. Kessentini, M. Belhouchet, Y. Abid, C. Minot, T. Mhiri, J. Spectro. Acta. PA. 122 (2014) 476-481.

[36] F. Harzi, Y. Arfaoui, C. Silvestru, N. Fakhar Bourguiba, Synthesis, structural and spectroscopic studies, DFT calculations, thermal characterization and Hirshfeld surface analysis of copper(II) organic-inorganic hybrid material $(C_{12}H_{22}N_2)[CuCl_4]$, J of coordination chemistry. 75 (2022) 70-83.

[37] R.S. Mulliken, A new electroaffinity scale; together with data on valence states and on valence ionization potentials and electron affinities, J. Chem. Phys. 2 (1934) 782–794.

[38] R.G. Parr, L. von Szentpály, S. Liu, Electrophilicity index, J. Am. Chem. Soc. 121 (1999) 1922–1924.

[39] K. Autumn, and al., Proc. Natl. Acad. Sci. U.S.A. 117 (792) (1995) 99, 12252 _2002; R. L. Baldwin, J. Mol. Biol. 371, 283 2007; P. Hobza et al.J. Am. Chem. Soc.

[40] A.C. Dillon, and al, Nature London 386 (377) (1997).

[41] E.R. Johnson, S. Keinan, P. Mori-Sánchez, J. Contreras-García, A.J. Cohen, W. Yang, J. Am. Chem. Soc. 132 (2010) 6498–6506.

[42] J. Contreras-Garcia, W. Yang, E.R. Johnson, Analysis of hydrogen-bond interaction potentials from the electron density: integration of non covalent interaction regions, J. Phys. Chem. A 115 (2011) 12983–12990.

[43] W. Humphrey, A. Dalke, K. Schulten, VMD: visual molecular dynamics, J. Mol. Graph. 14 (1996) 33–38 and 27-8.

[44] T. Lu, F. Chen, Multiwfn: a multifunctional wavefunction analyzer, J. Comput. Chem. 33 (2012) 580–592.

[45] R.F.W. Bader, Atoms in Molecules. A Quantum Theory, Oxford University Press, Oxford, 1990 0198558651.

[46] I. Rozas, I. Alkorta, J. Elguero, J. Am. Chem. Soc. 122 (2000) 11154 – 11161.

[47] C. Doghar, N. Issaoui, T. Roisnel, V. Dorcet, J. Mol. Struct, 1230 (2021), 129820.

[48] Christophe Morell, Andre´ Grand, Alejandro Toro-Labbe, J. Phys. Chem. A 109 (2005) 205–212.

[49] G.M. Morris, R. Huey, W. Lindstrom, M.F. Sanner, R.K. Belew, D.S. Goodsell, A.J. Olson, AutoDock4 and AutoDockTools4: automated docking with selective receptor flexibility, J. Comput. Chem. 30 (2009) 2785–2791.

[50] H. Marshan Robert, D Usha, M. Amalanathan, R. Racil Jeya Geetha, M. Sony Michael Mary, Vibrational spectral, density functional theory and molecular docking analysis on 4-nitrobenzohydrazide, Journal of Molecular Structure. 1223 (2021) 128948

[51] I. Jomaa, O. Noureddine, S. Gatfaoui, N. Issaoui, T. Roisnel, H. Marouani, Experimental, computational, and in silico analysis of $(C_8H_{14}N_2)_2[CdCl_6]$ compound, Journal of Molecular Structure. 1213 (2020) 128186.

data_AG21_02

#--#

Date of experiment: 03 fevrier 2021

#--#

#--#

CHEMICAL INFORMATION

#--#

_chemical_name_systematic

;

?

;

_chemical_formula_moiety 'C9 H15 N3, Cl4 Cu H2 O'

_chemical_formula_sum 'C9 H17 Cl4 Cu N3 O'

_chemical_formula_weight 388.59

_chemical_compound_source 'synthesis as described'

#--#

SPACE GROUP AND UNIT CELL INFORMATION

#--#

_space_group_crystal_system monoclinic

```
_space_group_name_H-M_alt              'P 21/n'
_space_group_name_Hall                 '-P 2yn'
_space_group_IT_number                  14
loop_
  _space_group_symop_operation_xyz
 'x, y, z'
 '-x+1/2, y+1/2, -z+1/2'
 '-x, -y, -z'
 'x-1/2, -y-1/2, z-1/2'

_cell_length_a                    10.2986(8)
_cell_length_b                    19.1385(13)
_cell_length_c                    7.6985(5)
_cell_angle_alpha                  90
_cell_angle_beta                   90.139(4)
_cell_angle_gamma                    90
_cell_volume                      1517.37(19)
_cell_formula_units_Z               4
_cell_measurement_temperature       296(2)
_cell_measurement_reflns_used       3388
_cell_measurement_theta_min         2.8519
_cell_measurement_theta_max         27.1497
_cell_measurement_wavelength        0.710730

#------------------------------------------------------------------------#
#                      ORIENTATION MATRIX                                #
```

#---#

_diffrn_orient_matrix_UB_11 0.0541924

_diffrn_orient_matrix_UB_21 -0.0732455

_diffrn_orient_matrix_UB_31 -0.0335677

_diffrn_orient_matrix_UB_12 -0.0395683

_diffrn_orient_matrix_UB_22 -0.0152957

_diffrn_orient_matrix_UB_32 -0.0305046

_diffrn_orient_matrix_UB_13 0.0442342

_diffrn_orient_matrix_UB_23 0.0760923

_diffrn_orient_matrix_UB_33 -0.0955319

#---#

CRYSTAL INFORMATION

#---#

_exptl_crystal_description prism

_exptl_crystal_colour green

_exptl_crystal_size_max 0.510

_exptl_crystal_size_mid 0.440

_exptl_crystal_size_min 0.190

_exptl_crystal_density_meas ?

_exptl_crystal_density_diffrn 1.701

_exptl_crystal_density_method ?

_exptl_crystal_F_000 788

_exptl_special_details

;

?

;

#---#

ABSORPTION CORRECTION

#---#

_exptl_absorpt_coefficient_mu 2.135

_exptl_absorpt_correction_type multi-scan

_exptl_absorpt_process_details

;

[Sheldrick, G.M. (2014). SADABS Bruker AXS Inc., Madison, Wisconsin, USA]

;

_exptl_absorpt_correction_T_min 0.494

_exptl_absorpt_correction_T_max 0.667

#---#

DATA COLLECTION

#---#

Software : BIS 2014.5.0.0/23-May-2014 && APEX2_2014.11-0

Number of scans : 2

Total number of frames : 201

Total length of scans : 201.00 (deg.)

Rotation speed : 8.00 sec./deg.

Total exposition time : 26.8 min.

```
#                                                                      #
#   Scan  Time(s)  Width  DX (mm)  Frames  Theta  Omega   Phi    Chi   T(K)  #
#.....................................................................#
#                                                                      #
#  1 Omega     8.0   1.00     35.0      93 343.95 350.71 333.14 316.27 299.26  #
#  2 Omega     8.0   1.00     35.0     108  16.05  14.52 101.73 304.12 299.26  #
#                                                                      #
#.....................................................................#

_diffrn_measurement_device_type         'APEXII Bruker-AXS'
_diffrn_measurement_method              'CCD rotation images, thin slices'
_diffrn_detector                        'CCD plate'
_diffrn_detector_area_resol_mean        8.33
_diffrn_ambient_temperature             296(2)
_diffrn_radiation_wavelength            0.71073
_diffrn_radiation_type                  MoK\a
_diffrn_radiation_probe                 x-ray
_diffrn_radiation_source                'fine-focus sealed tube'
_diffrn_radiation_monochromator         graphite
_diffrn_reflns_av_uneti/neti            0.0513
_diffrn_reflns_av_r_equivalents         0.0329
_diffrn_reflns_number                   7420
_diffrn_reflns_limit_h_min              -13
_diffrn_reflns_limit_h_max              9
_diffrn_reflns_limit_k_min              -15
_diffrn_reflns_limit_k_max              24
_diffrn_reflns_limit_l_min              -9
```

_diffrn_reflns_limit_l_max 9

_diffrn_reflns_theta_min 1.977

_diffrn_reflns_theta_max 27.470

_diffrn_reflns_theta_full 25.242

_diffrn_measured_fraction_theta_full 0.994

_diffrn_measured_fraction_theta_max 0.993

_reflns_number_total 3444

_reflns_number_gt 3004

_reflns_threshold_expression >2sigma(I)

_reflns_special_details

;

Reflections were merged by SHELXL according to the crystal class for the calculation of statistics and refinement.

;

#----------#

COMPUTER PROGRAMS USED

#----------#

_computing_data_collection 'Bruker APEX2 (Bruker, 2014)'

_computing_cell_refinement 'Bruker APEX2 (Bruker, 2014)'

_computing_data_reduction 'Bruker APEX2 (Bruker, 2014)'

_computing_structure_solution 'SHELXT 2018_2 (Sheldrick, 2018)'

_computing_structure_refinement 'SHELXL-2018_3 (Sheldrick, 2018)'

_computing_molecular_graphics

;

'SXGRAPH (L. Farrugia, 1999), Mercury (CSD, 2020)'

;

_computing_publication_material 'CRYSCALC (T. Roisnel, local program, ver. 2021)'

#---#

REFINEMENT INFORMATION

#---#

_refine_special_details

;

Refinement of F^2^ against ALL reflections. The weighted R-factor wR and goodness of fit S are based on F^2^, conventional R-factors R are based on F, with F set to zero for negative F^2^. The threshold expression of F^2^ > 2sigma(F^2^) is used only for calculating R-factors(gt) etc. and is not relevant to the choice of reflections for refinement. R-factors based on F^2^ are statistically about twice as large as those based on F, and R-factors based on ALL data will be even larger.

;

_refine_ls_structure_factor_coef Fsqd

_refine_ls_matrix_type full

_refine_ls_weighting_scheme calc

_refine_ls_weighting_details

'w=1/[\s^2^(Fo^2^)+(0.0339P)^2^] where P=(Fo^2^+2Fc^2^)/3'

_atom_sites_solution_primary dual

_atom_sites_solution_secondary difmap

_atom_sites_solution_hydrogens mixed

```
_refine_ls_hydrogen_treatment          mixed
_refine_ls_extinction_method           none
_refine_ls_extinction_coef             .
_refine_ls_number_reflns               3444
_refine_ls_number_parameters           179
_refine_ls_number_restraints           2
_refine_ls_R_factor_all                0.0421
_refine_ls_R_factor_gt                 0.0345
_refine_ls_wR_factor_ref               0.0825
_refine_ls_wR_factor_gt                0.0795
_refine_ls_goodness_of_fit_ref         1.044
_refine_ls_restrained_S_all            1.045
_refine_ls_shift/su_max                0.000
_refine_ls_shift/su_mean               0.000
_refine_diff_density_max               0.561
_refine_diff_density_min               -0.352
_refine_diff_density_rms               0.072

#-------------------------------------------------------------------------------#
#            ATOMIC TYPES, COORDINATES AND THERMAL PARAMETERS                   #
#-------------------------------------------------------------------------------#

loop_
   _atom_type_symbol
   _atom_type_description
   _atom_type_scat_dispersion_real
   _atom_type_scat_dispersion_imag
```

```
   _atom_type_scat_source
C   C    0.0033  0.0016  'International Tables Vol C Tables 4.2.6.8 and 6.1.1.4'
H   H    0.0000  0.0000  'International Tables Vol C Tables 4.2.6.8 and 6.1.1.4'
N   N    0.0061  0.0033  'International Tables Vol C Tables 4.2.6.8 and 6.1.1.4'
Cu  Cu   0.3201  1.2651  'International Tables Vol C Tables 4.2.6.8 and 6.1.1.4'
Cl  Cl   0.1484  0.1585  'International Tables Vol C Tables 4.2.6.8 and 6.1.1.4'
O   O    0.0106  0.0060  'International Tables Vol C Tables 4.2.6.8 and 6.1.1.4'

loop_
   _atom_site_label
   _atom_site_type_symbol
   _atom_site_fract_x
   _atom_site_fract_y
   _atom_site_fract_z
   _atom_site_U_iso_or_equiv
   _atom_site_adp_type
   _atom_site_occupancy
   _atom_site_site_symmetry_order
   _atom_site_calc_flag
   _atom_site_refinement_flags_posn
   _atom_site_refinement_flags_adp
   _atom_site_refinement_flags_occupancy
   _atom_site_disorder_assembly
   _atom_site_disorder_group
Cu1  Cu  0.49215(4)   0.11560(2)   0.21791(5)   0.02525(11) Uani 1 1 d    .    . . . .
Cl1  Cl  0.59337(9)   0.08838(4)   0.47871(11)  0.0376(2)   Uani 1 1 d    .    . . . .
Cl2  Cl  0.68189(7)   0.11167(4)   0.00606(11)  0.03068(19) Uani 1 1 d    .    . . . .
```

Cl3 Cl 0.49768(10) 0.23117(4) 0.28087(10) 0.0398(2) Uani 1 1 d . . . .

Cl4 Cl 0.33326(8) 0.12840(4) 0.01222(12) 0.0342(2) Uani 1 1 d . . . .

OW1 O 0.4622(3) 0.01277(12) 0.2025(3) 0.0522(9) Uani 1 1 d D . . .

H1A H 0.415(3) -0.0079(17) 0.122(4) 0.050 Uiso 1 1 d D . . .

H1B H 0.478(4) -0.0125(18) 0.299(4) 0.050 Uiso 1 1 d D . . .

C11 C 0.6141(3) 0.46850(17) 0.8303(4) 0.0314(7) Uani 1 1 d . . . .

H11 H 0.691338 0.450894 0.875310 0.038 Uiso 1 1 calc R U . . .

C12 C 0.6040(4) 0.53748(18) 0.7929(5) 0.0385(8) Uani 1 1 d . . . .

H12 H 0.674658 0.566682 0.813079 0.046 Uiso 1 1 calc R U . . .

C13 C 0.4903(4) 0.56537(18) 0.7250(4) 0.0455(9) Uani 1 1 d . . . .

H13 H 0.483275 0.612914 0.701809 0.055 Uiso 1 1 calc R U . . .

C14 C 0.3906(4) 0.52176(18) 0.6935(5) 0.0453(10) Uani 1 1 d . . . .

H14 H 0.314219 0.539100 0.645537 0.054 Uiso 1 1 calc R U . . .

N15 N 0.4005(3) 0.45269(14) 0.7312(4) 0.0331(7) Uani 1 1 d . . . .

H15 H 0.334(3) 0.4317(19) 0.706(5) 0.040 Uiso 1 1 d . U . . .

C16 C 0.5074(3) 0.42295(16) 0.8013(4) 0.0258(6) Uani 1 1 d . . . .

N17 N 0.5056(3) 0.35487(13) 0.8410(3) 0.0300(6) Uani 1 1 d . . . .

C18 C 0.3880(3) 0.31209(16) 0.8493(4) 0.0265(7) Uani 1 1 d . . . .

H18A H 0.312302 0.341668 0.833969 0.032 Uiso 1 1 calc R U . . .

H18B H 0.382176 0.290260 0.962706 0.032 Uiso 1 1 calc R U . . .

C19 C 0.3889(3) 0.25662(16) 0.7112(4) 0.0307(7) Uani 1 1 d . . . .

H19A H 0.312518 0.227315 0.722145 0.037 Uiso 1 1 calc R U . . .

H19B H 0.387569 0.278131 0.597133 0.037 Uiso 1 1 calc R U . . .

N20 N 0.5080(3) 0.21364(15) 0.7315(4) 0.0332(6) Uani 1 1 d . . . .

H20A H 0.510(4) 0.1856(18) 0.651(4) 0.040 Uiso 1 1 d . U . . .

H20B H 0.507(4) 0.1928(17) 0.835(4) 0.040 Uiso 1 1 d . U . . .

C21 C 0.6294(3) 0.25666(16) 0.7315(5) 0.0314(7) Uani 1 1 d . . . .

H21A H 0.640876 0.277918 0.618153 0.038 Uiso 1 1 calc R U . . .

H21B H 0.703708 0.226824 0.754060 0.038 Uiso 1 1 calc R U . . .

C22 C 0.6224(3) 0.31264(17) 0.8676(4) 0.0321(8) Uani 1 1 d . . . . .

H22A H 0.620244 0.291483 0.982008 0.039 Uiso 1 1 calc R U . . .

H22B H 0.698765 0.342152 0.860742 0.039 Uiso 1 1 calc R U . . .

loop_

_atom_site_aniso_label

_atom_site_aniso_U_11

_atom_site_aniso_U_22

_atom_site_aniso_U_33

_atom_site_aniso_U_23

_atom_site_aniso_U_13

_atom_site_aniso_U_12

Cu1 0.0296(2) 0.02279(18) 0.02336(19) 0.00033(14) 0.0016(2) -0.00237(16)

Cl1 0.0518(5) 0.0320(4) 0.0289(4) 0.0056(3) -0.0075(4) -0.0059(4)

Cl2 0.0237(4) 0.0412(4) 0.0272(4) -0.0013(4) 0.0023(3) 0.0027(3)

Cl3 0.0637(6) 0.0239(4) 0.0316(4) -0.0020(3) -0.0023(5) -0.0003(4)

Cl4 0.0274(4) 0.0371(4) 0.0382(5) -0.0001(4) -0.0046(4) -0.0016(3)

OW1 0.091(3) 0.0270(13) 0.0383(15) 0.0047(11) -0.0221(16) -0.0184(14)

C11 0.0277(17) 0.0376(18) 0.0290(17) -0.0030(15) 0.0046(14) -0.0046(15)

C12 0.040(2) 0.0391(19) 0.0369(19) -0.0042(17) 0.0080(18) -0.0150(17)

C13 0.066(2) 0.0258(16) 0.045(2) 0.0043(15) -0.001(2) -0.0063(19)

C14 0.051(2) 0.0361(19) 0.048(2) 0.0082(18) -0.011(2) 0.0069(19)

N15 0.0321(15) 0.0300(15) 0.0373(16) -0.0013(13) -0.0087(14) -0.0010(13)

C16 0.0248(14) 0.0310(15) 0.0216(14) -0.0051(12) 0.0015(14) 0.0007(14)

N17 0.0192(12) 0.0282(13) 0.0426(14) -0.0012(12) 0.0010(14) 0.0008(12)

C18 0.0201(15) 0.0271(16) 0.0324(18) 0.0013(14) 0.0063(14) -0.0005(13)

C19 0.0245(15) 0.0323(16) 0.0352(18) 0.0009(16) -0.0004(15) 0.0023(14)

N20 0.0325(15) 0.0271(14) 0.0400(16) 0.0007(12) 0.0080(17) 0.0004(13)

C21 0.0225(15) 0.0309(16) 0.041(2) 0.0052(16) 0.0078(15) 0.0028(13)

C22 0.0240(16) 0.0341(18) 0.038(2) 0.0015(15) -0.0049(15) 0.0019(15)

#---#

MOLECULAR GEOMETRY

#---#

_geom_special_details

;

All esds (except the esd in the dihedral angle between two l.s. planes)

are estimated using the full covariance matrix. The cell esds are taken

into account individually in the estimation of esds in distances, angles

and torsion angles; correlations between esds in cell parameters are only

used when they are defined by crystal symmetry. An approximate (isotropic)

treatment of cell esds is used for estimating esds involving l.s. planes.

;

loop_

_geom_bond_atom_site_label_1

_geom_bond_atom_site_label_2

_geom_bond_distance

_geom_bond_site_symmetry_2

_geom_bond_publ_flag

Cu1 OW1 1.996(2) . ?

Cu1 Cl3 2.2650(8) . ?

Cu1 Cl4 2.2875(9) . ?

Cu1 Cl1 2.3193(9) . ?

Cu1 Cl2 2.5494(9) . ?

OW1 H1A 0.89(2) . ?

OW1 H1B 0.90(2) . ?

C11 C12 1.355(5) . ?

C11 C16 1.420(4) . ?

C11 H11 0.9300 . ?

C12 C13 1.388(5) . ?

C12 H12 0.9300 . ?

C13 C14 1.344(5) . ?

C13 H13 0.9300 . ?

C14 N15 1.357(4) . ?

C14 H14 0.9300 . ?

N15 C16 1.351(4) . ?

N15 H15 0.82(3) . ?

C16 N17 1.338(4) . ?

N17 C22 1.463(4) . ?

N17 C18 1.464(4) . ?

C18 C19 1.502(4) . ?

C18 H18A 0.9700 . ?

C18 H18B 0.9700 . ?

C19 N20 1.485(4) . ?

C19 H19A 0.9700 . ?

C19 H19B 0.9700 . ?

N20 C21 1.497(4) . ?

N20 H20A 0.82(3) . ?

N20 H20B 0.89(3) . ?

C21 C22 1.501(4) . ?

C21 H21A 0.9700 . ?

C21 H21B 0.9700 . ?

C22 H22A 0.9700 . ?

C22 H22B 0.9700 . ?

loop_

_geom_angle_atom_site_label_1

_geom_angle_atom_site_label_2

_geom_angle_atom_site_label_3

_geom_angle

_geom_angle_site_symmetry_1

_geom_angle_site_symmetry_3

_geom_angle_publ_flag

OW1 Cu1 Cl3 168.40(9) . . ?

OW1 Cu1 Cl4 87.36(8) . . ?

Cl3 Cu1 Cl4 93.51(3) . . ?

OW1 Cu1 Cl1 84.22(8) . . ?

Cl3 Cu1 Cl1 91.32(3) . . ?

Cl4 Cu1 Cl1 160.49(4) . . ?

OW1 Cu1 Cl2 92.95(9) . . ?

Cl3 Cu1 Cl2 98.44(3) . . ?

Cl4 Cu1 Cl2 96.23(3) . . ?

Cl1 Cu1 Cl2 101.75(3) . . ?

Cu1 OW1 H1A 125(2) . . ?

Cu1 OW1 H1B 117(2) . . ?

H1A OW1 H1B 116(3) . . ?

C12 C11 C16 120.4(3) . . ?

C12 C11 H11 119.8 . . ?

C16 C11 H11 119.8 . . ?

C11 C12 C13 121.2(3) . . ?

C11 C12 H12 119.4 . . ?

C13 C12 H12 119.4 . . ?

C14 C13 C12 118.2(3) . . ?

C14 C13 H13 120.9 . . ?

C12 C13 H13 120.9 . . ?

C13 C14 N15 120.7(3) . . ?

C13 C14 H14 119.7 . . ?

N15 C14 H14 119.7 . . ?

C16 N15 C14 123.8(3) . . ?

C16 N15 H15 125(3) . . ?

C14 N15 H15 111(3) . . ?

N17 C16 N15 119.3(3) . . ?

N17 C16 C11 125.0(3) . . ?

N15 C16 C11 115.7(3) . . ?

C16 N17 C22 123.9(3) . . ?

C16 N17 C18 124.5(3) . . ?

C22 N17 C18 111.4(2) . . ?

N17 C18 C19 110.9(3) . . ?

N17 C18 H18A 109.4 . . ?

C19 C18 H18A 109.4 . . ?

N17 C18 H18B 109.4 . . ?

C19 C18 H18B 109.4 . . ?

H18A C18 H18B 108.0 . . ?

N20 C19 C18 108.9(3) . . ?

N20 C19 H19A 109.9 . . ?

C18 C19 H19A 109.9 . . ?

N20 C19 H19B 109.9 . . ?

C18 C19 H19B 109.9 . . ?

H19A C19 H19B 108.3 . . ?

C19 N20 C21 112.6(2) . . ?

C19 N20 H20A 108(3) . . ?

C21 N20 H20A 110(3) . . ?

C19 N20 H20B 110(3) . . ?

C21 N20 H20B 105(2) . . ?

H20A N20 H20B 112(3) . . ?

N20 C21 C22 110.5(3) . . ?

N20 C21 H21A 109.5 . . ?

C22 C21 H21A 109.5 . . ?

N20 C21 H21B 109.5 . . ?

C22 C21 H21B 109.5 . . ?

H21A C21 H21B 108.1 . . ?

N17 C22 C21 109.8(2) . . ?

N17 C22 H22A 109.7 . . ?

C21 C22 H22A 109.7 . . ?

N17 C22 H22B 109.7 . . ?

C21 C22 H22B 109.7 . . ?

H22A C22 H22B 108.2 . . ?

```
loop_
   _geom_torsion_atom_site_label_1
   _geom_torsion_atom_site_label_2
   _geom_torsion_atom_site_label_3
   _geom_torsion_atom_site_label_4
   _geom_torsion
   _geom_torsion_site_symmetry_1
   _geom_torsion_site_symmetry_2
   _geom_torsion_site_symmetry_3
   _geom_torsion_site_symmetry_4
   _geom_torsion_publ_flag
C16  C11  C12  C13    -0.3(5)    .    .    .    .    ?
C11  C12  C13  C14    -1.4(6)    .    .    .    .    ?
C12  C13  C14  N15     1.5(6)    .    .    .    .    ?
C13  C14  N15  C16     0.1(6)    .    .    .    .    ?
C14  N15  C16  N17   177.0(3)    .    .    .    .    ?
C14  N15  C16  C11    -1.7(5)    .    .    .    .    ?
C12  C11  C16  N17  -176.9(3)    .    .    .    .    ?
C12  C11  C16  N15     1.8(5)    .    .    .    .    ?
N15  C16  N17  C22   161.1(3)    .    .    .    .    ?
C11  C16  N17  C22   -20.3(5)    .    .    .    .    ?
N15  C16  N17  C18   -13.7(4)    .    .    .    .    ?
C11  C16  N17  C18   164.9(3)    .    .    .    .    ?
C16  N17  C18  C19   114.9(3)    .    .    .    .    ?
C22  N17  C18  C19   -60.5(3)    .    .    .    .    ?
N17  C18  C19  N20    56.7(3)    .    .    .    .    ?
C18  C19  N20  C21   -54.6(4)    .    .    .    .    ?
```

```
C19  N20  C21  C22    54.8(3)    .      .      .      .      ?
C16  N17  C22  C21  -116.3(3)    .      .      .      .      ?
C18  N17  C22  C21    59.0(3)    .      .      .      .      ?
N20  C21  C22  N17   -55.4(4)    .      .      .      .      ?

loop_
   _geom_hbond_atom_site_label_D
   _geom_hbond_atom_site_label_H
   _geom_hbond_atom_site_label_A
   _geom_hbond_distance_DH
   _geom_hbond_distance_HA
   _geom_hbond_distance_DA
   _geom_hbond_angle_DHA
   _geom_hbond_site_symmetry_A
   _geom_hbond_publ_flag
#
# Hydrogen bonding scheme
# ----------------------
#
# D      H      A      D-H        H...A      D...A      D-H...A   symm publ
# ------------------------------------------------------------------------------
 OW1    H1A    Cl2    0.89(2)    2.43(3)    3.231(3)   151(3)    3_655 yes
 OW1    H1B    Cl1    0.90(2)    2.36(3)    3.179(3)   151(3)    3_656 yes
 C14    H14    Cl4    0.93       2.59       3.460(4)   156.6     2     yes
 N15    H15    Cl2    0.82(3)    2.34(4)    3.093(3)   153(4)    4_566 yes
 C19    H19B   Cl3    0.97       2.83       3.533(4)   129.7     .     yes
 N20    H20A   Cl1    0.82(3)    2.44(4)    3.212(3)   157(3)    .     yes
```

N20	H20B	Cl2	0.89(3)	2.71(4)	3.386(3)	133(3)	1_556 yes
N20	H20B	Cl4	0.89(3)	2.57(4)	3.254(3)	134(3)	1_556 yes
C21	H21A	Cl4	0.97	2.80	3.480(3)	128.3	4_666 yes

#--#

EMBEDDED FILES

#--#

# #

#.....

.RES SHELXL file: job.res

#.....

_shelx_res_file

;

TITL AG21 [Space group= P2(1)/n]

job.res

created by SHELXL-2018/3 at 12:44:28 on 03-Feb-2021

CELL 0.71073 10.2986 19.1385 7.6985 90.000 90.139 90.000

ZERR 4.00 0.0008 0.0013 0.0005 0.000 0.004 0.000

LATT 1

SYMM 1/2 - X, 1/2 + Y, 1/2 - Z

SFAC C H N CU CL O

UNIT 36 68 12 4 16 4

MERG 2

OMIT 1 1 0

TWIN 1.00 0.00 0.01 0.00 -1.00 0.00 0.00 0.00 -1.00 2

DFIX 0.95 0.03 Ow1 H1a

DFIX 0.95 0.03 Ow1 H1b

EQIV $1 -x+1, -y, -z

HTAB OW1 Cl2_$1

EQIV $2 -x+1, -y, -z+1

HTAB OW1 Cl1_$2

EQIV $3 -x+1/2, y+1/2, -z+1/2

HTAB C14 Cl4_$3

EQIV $4 x-1/2, -y+1/2, z+1/2

HTAB N15 Cl2_$4

HTAB C18 Cl1_$4

EQIV $5 x, y, z+1

HTAB C18 Cl3_$5

HTAB C19 Cl4_$5

HTAB C19 Cl3

HTAB N20 Cl1

HTAB N20 Cl3

HTAB N20 Cl2_$5

HTAB N20 Cl4_$5

EQIV $6 x+1/2, -y+1/2, z+1/2

HTAB C21 Cl4_$6

HTAB C21 Cl2_$5

HTAB C22 Cl3_$5

FMAP 2

PLAN 20

SIZE 0.19 0.44 0.51

ACTA

```
HTAB    2.00000
BOND   $H
CONF
LIST   4
WPDB  -2
L.S.   4
TEMP    23.00
WGHT    0.033900
BASF   0.25396
FVAR       0.35175
MOLE    1
CU1   4    0.492147    0.115601    0.217911    11.00000    0.02961    0.02279 =
      0.02336    0.00033    0.00156   -0.00237
CL1   5    0.593371    0.088381    0.478714    11.00000    0.05183    0.03198 =
      0.02887    0.00556   -0.00747   -0.00586
CL2   5    0.681888    0.111667    0.006063    11.00000    0.02366    0.04117 =
      0.02721   -0.00131    0.00228    0.00272
CL3   5    0.497676    0.231173    0.280872    11.00000    0.06371    0.02393 =
      0.03165   -0.00197   -0.00233   -0.00034
CL4   5    0.333255    0.128396    0.012223    11.00000    0.02735    0.03713 =
      0.03822   -0.00009   -0.00461   -0.00155
OW1   6    0.462164    0.012768    0.202464    11.00000    0.09128    0.02695 =
      0.03833    0.00470   -0.02210   -0.01840
AFIX   2
H1A   2    0.414532   -0.007916    0.121546    11.00000    0.05000
H1B   2    0.477937   -0.012452    0.299325    11.00000    0.05000
AFIX   0
```

MOLE 2

C11 1 0.614099 0.468500 0.830321 11.00000 0.02771 0.03761 =

0.02896 -0.00301 0.00461 -0.00463

AFIX 43

H11 2 0.691338 0.450894 0.875310 11.00000 -1.20000

AFIX 0

C12 1 0.604041 0.537479 0.792883 11.00000 0.03961 0.03914 =

0.03688 -0.00422 0.00795 -0.01495

AFIX 43

H12 2 0.674658 0.566682 0.813079 11.00000 -1.20000

AFIX 0

C13 1 0.490321 0.565371 0.724955 11.00000 0.06598 0.02581 =

0.04474 0.00427 -0.00087 -0.00629

AFIX 43

H13 2 0.483275 0.612914 0.701809 11.00000 -1.20000

AFIX 0

C14 1 0.390648 0.521759 0.693550 11.00000 0.05147 0.03607 =

0.04832 0.00818 -0.01141 0.00690

AFIX 43

H14 2 0.314219 0.539100 0.645537 11.00000 -1.20000

AFIX 0

N15 3 0.400456 0.452692 0.731211 11.00000 0.03207 0.02999 =

0.03728 -0.00126 -0.00869 -0.00100

AFIX 2

H15 2 0.333813 0.431718 0.706050 11.00000 -1.20000

AFIX 0

C16 1 0.507412 0.422948 0.801268 11.00000 0.02482 0.03101 =

0.02157 -0.00509 0.00150 0.00073

N17 3 0.505591 0.354874 0.840970 11.00000 0.01919 0.02817 =

0.04262 -0.00117 0.00098 0.00077

C18 1 0.387960 0.312095 0.849282 11.00000 0.02010 0.02705 =

0.03239 0.00133 0.00631 -0.00053

AFIX 23

H18A 2 0.312302 0.341668 0.833969 11.00000 -1.20000

H18B 2 0.382176 0.290260 0.962706 11.00000 -1.20000

AFIX 0

C19 1 0.388910 0.256620 0.711210 11.00000 0.02446 0.03232 =

0.03520 0.00091 -0.00043 0.00235

AFIX 23

H19A 2 0.312518 0.227315 0.722145 11.00000 -1.20000

H19B 2 0.387569 0.278131 0.597133 11.00000 -1.20000

AFIX 0

N20 3 0.508026 0.213635 0.731544 11.00000 0.03253 0.02708 =

0.04004 0.00071 0.00803 0.00041

AFIX 2

H20A 2 0.510083 0.185636 0.651051 11.00000 -1.20000

H20B 2 0.507336 0.192762 0.834692 11.00000 -1.20000

AFIX 0

C21 1 0.629420 0.256655 0.731459 11.00000 0.02253 0.03094 =

0.04062 0.00520 0.00781 0.00281

AFIX 23

H21A 2 0.640876 0.277918 0.618153 11.00000 -1.20000

H21B 2 0.703708 0.226824 0.754060 11.00000 -1.20000

AFIX 0

C22 1 0.622370 0.312643 0.867557 11.00000 0.02396 0.03413 =

0.03815 0.00148 -0.00488 0.00190

AFIX 23

H22A 2 0.620244 0.291483 0.982008 11.00000 -1.20000

H22B 2 0.698765 0.342152 0.860742 11.00000 -1.20000

AFIX 0

HKLF 4

REM AG21 [Space group= P2(1)/n]

REM wR2 = 0.0825, GooF = S = 1.044, Restrained GooF = 1.045 for all data

REM R1 = 0.0345 for 3004 Fo > 4sig(Fo) and 0.0421 for all 3444 data

REM 179 parameters refined using 2 restraints

END

WGHT 0.0339 0.0000

REM Instructions for potential hydrogen bonds

HTAB OW1 Cl2_$1

HTAB OW1 Cl1_$2

HTAB C14 Cl4_$3

HTAB N15 Cl2_$4

HTAB C18 Cl1_$4

HTAB C18 Cl3_$5

HTAB C19 Cl4_$5

HTAB C19 Cl3

HTAB N20 Cl1

HTAB N20 Cl3

HTAB N20 Cl2_$5

HTAB N20 Cl4_$5

HTAB C21 Cl4_$6

HTAB C21 Cl2_$5

HTAB C22 Cl3_$5

REM Highest difference peak 0.561, deepest hole -0.352, 1-sigma level 0.072

Q1 1 0.5195 0.0891 0.5017 11.00000 0.05 0.56

Q2 1 0.4247 0.0896 0.5156 11.00000 0.05 0.50

Q3 1 0.2859 0.1160 0.0453 11.00000 0.05 0.41

Q4 1 0.6346 0.1351 0.0601 11.00000 0.05 0.31

Q5 1 0.5678 0.2264 0.2947 11.00000 0.05 0.30

Q6 1 0.3857 0.1020 -0.0292 11.00000 0.05 0.30

Q7 1 0.5617 0.4424 0.8039 11.00000 0.05 0.27

Q8 1 0.5842 0.2367 0.7338 11.00000 0.05 0.25

Q9 1 0.2984 0.0902 -0.0591 11.00000 0.05 0.25

Q10 1 0.6815 0.0616 0.0201 11.00000 0.05 0.25

Q11 1 0.3137 0.1028 -0.0787 11.00000 0.05 0.24

Q12 1 0.7003 0.1523 -0.0323 11.00000 0.05 0.24

Q13 1 0.5011 0.1736 0.2451 11.00000 0.05 0.24

Q14 1 0.3631 0.0861 0.0414 11.00000 0.05 0.23

Q15 1 0.6497 0.2707 0.6538 11.00000 0.05 0.23

Q16 1 0.7375 0.1145 -0.0012 11.00000 0.05 0.23

Q17 1 0.3125 0.1764 -0.0229 11.00000 0.05 0.23

Q18 1 0.6755 0.1539 0.0346 11.00000 0.05 0.22

Q19 1 0.3755 0.0759 0.2541 11.00000 0.05 0.21

Q20 1 0.3349 0.5287 0.6999 11.00000 0.05 0.21

checkCIF/PLATON report

Structure factors have been supplied for datablock(s) AG21_02
THIS REPORT IS FOR GUIDANCE ONLY. IF USED AS PART OF A REVIEW PROCEDURE FOR
PUBLICATION, IT SHOULD NOT REPLACE THE EXPERTISE OF AN EXPERIENCED CRYSTALLOGRAPHIC REFEREE.
No syntax errors found. CIF dictionary Interpreting this report

Datablock: AG21_02

```
Bond precision: C-C = 0.0048 A Wavelength=0.71073
Cell: a=10.2986(8) b=19.1385(13) c=7.6985(5)
alpha=90 beta=90.139(4) gamma=90
Temperature: 296 K
Calculated Reported
Volume 1517.37(19) 1517.37(19)
Space group P 21/n P 21/n
Hall group -P 2yn -P 2yn
Moiety formula C9 H15 N3, Cl4 Cu H2 O C9 H15 N3, Cl4 Cu H2 O
Sum formula C9 H17 Cl4 Cu N3 O C9 H17 Cl4 Cu N3 O
Mr 388.61 388.59
Dx,g cm-3 1.701 1.701
Z 4 4
Mu (mm-1) 2.135 2.135
F000 788.0 788.0
F000' 791.78
h,k,lmax 13,24,9 13,24,9
Nref 3470 3444
Tmin,Tmax 0.350,0.667 0.494,0.667
Tmin' 0.324
Correction method= # Reported T Limits: Tmin=0.494 Tmax=0.667
AbsCorr = MULTI-SCAN
Data completeness= 0.993 Theta(max)= 27.470
R(reflections)= 0.0345( 3004)
wR2(reflections)=
0.0825( 3444)
S = 1.044 Npar= 179
```

The following ALERTS were generated. Each ALERT has the format
test-name_ALERT_alert-type_alert-level.
Click on the hyperlinks for more details of the test.

Alert level C

PLAT911_ALERT_3_C Missing FCF Refl Between Thmin & STh/L= 0.600 15 Report

Alert level G

PLAT002_ALERT_2_G Number of Distance or Angle Restraints on AtSite 3 Note
PLAT158_ALERT_4_G The Input Unitcell is NOT Standard/Reduced ..... Please Check
PLAT172_ALERT_4_G The CIF-Embedded .res File Contains DFIX Records 2 Report
PLAT720_ALERT_4_G Number of Unusual/Non-Standard Labels ..... 1 Note
PLAT860_ALERT_3_G Number of Least-Squares Restraints ..... 2 Note
PLAT870_ALERT_4_G ALERTS Related to Twinning Effects Suppressed .. ! Info
PLAT910_ALERT_3_G Missing # of FCF Reflection(s) Below Theta(Min). 2 Note
PLAT912_ALERT_4_G Missing # of FCF Reflections Above STh/L= 0.600 9 Note
PLAT931_ALERT_5_G CIFcalcFCF Twin Law (0 0 1) Est.d BASF 0.25 Check
PLAT933_ALERT_2_G Number of HKL-OMIT Records in Embedded .res File 1 Note
PLAT941_ALERT_3_G Average HKL Measurement Multiplicity ..... 2.1 Low

0 **ALERT level A** = Most likely a serious problem - resolve or explain
0 **ALERT level B** = A potentially serious problem, consider carefully
1 **ALERT level C** = Check. Ensure it is not caused by an omission or oversight
11 **ALERT level G** = General information/check it is not something unexpected
0 ALERT type 1 CIF construction/syntax error, inconsistent or missing data
2 ALERT type 2 Indicator that the structure model may be wrong or deficient
4 ALERT type 3 Indicator that the structure quality may be low
5 ALERT type 4 Improvement, methodology, query or suggestion
1 ALERT type 5 Informative message, check

It is advisable to attempt to resolve as many as possible of the alerts in all categories. Often the minor alerts point to easily fixed oversights, errors and omissions in your CIF or refinement strategy, so attention to these fine details can be worthwhile. In order to resolve some of the more serious problems it may be necessary to carry out additional measurements or structure refinements. However, the purpose of your study may justify the reported deviations and the more serious of these should normally be commented upon in the discussion or experimental section of a paper or in the "special_details" fields of the CIF. checkCIF was carefully designed to identify outliers and unusual parameters, but every test has its limitations and alerts that are not important in a particular case may appear. Conversely, the absence of alerts does not guarantee there are no aspects of the results needing attention. It is up to the individual to critically assess their own results and, if necessary, seek expert advice.

Publication of your CIF in IUCr journals

A basic structural check has been run on your CIF. These basic checks will be run on all CIFs submitted for publication in IUCr journals (*Acta Crystallographica*, *Journal of Applied Crystallography*, *Journal of Synchrotron Radiation*); however, if you intend to submit to *Acta Crystallographica Section C* or *E* or *IUCrData*, you should make sure that full publication checks are run on the final version of your CIF prior to submission.

Publication of your CIF in other journals

Please refer to the *Notes for Authors* of the relevant journal for any special instructions relating to CIF
submission.

PLATON version of 18/05/2022; check.def file version of 17/05/2022

Datablock AG21_02 - ellipsoid plot

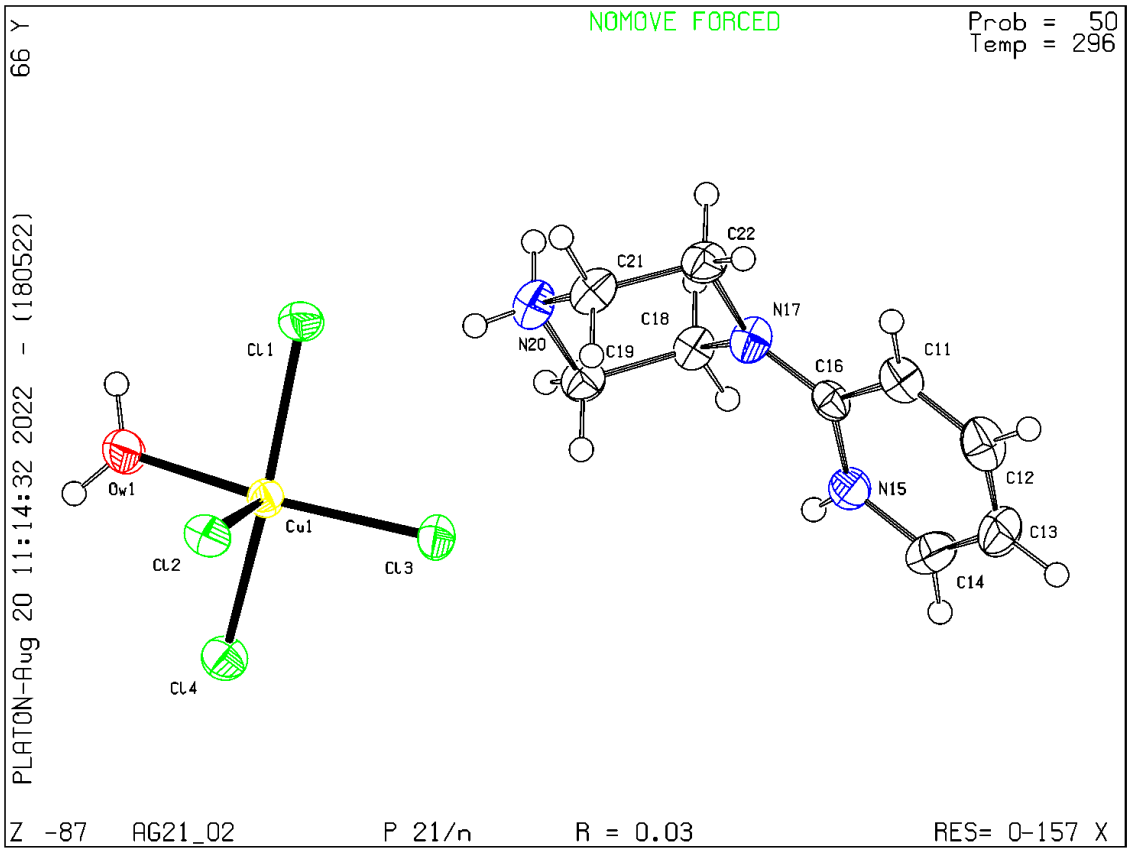

Highlights

- A New Organic-Inorganic Hybrid Compound $(C_9H_{15}N_3)[CuCl_4(H_2O)]$ was successfully synthesized and structurally characterized.
- Intermolecular interactions were explored using Hirshfeld surface analysis and RDG approach.
- Optical properties and vibrational bands of the compound were discussed and investigated by DFT calculations.
- Antibacterial activity of compound has been tested by DPPH and ABTS.
- Molecular docking studies confirmed the inhibitory activity of $(C_9H_{15}N_3)[CuCl_4(H_2O)]$.

X-Ray diffraction, IR spectrum, optical properties, AIM, NBO, RDG, HS, Fukui function, biological and molecular docking analysis of a novel hybrid compound ($C_9H_{15}N_3$)[$CuCl_4(H_2O)$]

Afef Gannouni[a], Wiem Tahri[b], Thierry Roisnel[c], Riadh Kefi[a]

[a]Laboratoire de Chimie des Matériaux, Faculté des Sciences de Bizerte, 7021 Zarzouna, Tunisie.
[b]Laboratory of Biochemistry and Molecular Biology, Faculty of Sciences, Risks Related to Environmental Stress, Struggle and Prevention (UR17ES20), University of Carthage, Te Ministry of Higher Education and Scientifc Research, Zarzouna, 7003 Bizerte, Tunisia.
[c]Univ Rennes, CNRS, ISCR (Institut des Sciences Chimiques de Rennes) – UMR 6226, F-35000 Rennes, France.

Figure caption

Fig. 1 (a) Asymmetric unit and atom labeling scheme of $(C_9H_{15}N_3)[CuCl_4(H_2O)]$, (b) optimized geometry of the cluster model used in the DFT and TDDFT calculations.

Fig. 2 A view of down b-axis of chains $\{[CuCl_4(H_2O)]^{2-}\}_n$ linkage by means O-H…Cl hydrogen bonds.

Fig. 3 Projection along the c-axis of $(C_9H_{15}N_3)[CuCl_4(H_2O)]$. The dotted lines indicate hydrogen bonds.

Fig. 4 (a) 2d fingerprint of the whole molecule (b) Hirshfeld surfaces mapped with d_{norm}, (c) Hirshfeld surface mapped with shape index and (d) curvedness of $(C_9H_{15}N_3)[CuCl_4(H_2O)]$.

Fig. 5 Experimental and theoretical FT-IR Spectra of $(C_9H_{15}N_3)[CuCl_4(H_2O)]$

Fig. 6 Energy dependence of $(F(R)\ h\nu)^2$ versus photon ($h\nu$) for $(C_9H_{15}N_3)[CuCl_4(H_2O)]$.

Fig. 7 Molecular orbital surfaces for the LUMO, LUMO+1, HOMO et HOMO-1 of $(C_9H_{15}N_3)[CuCl_4(H_2O)]$.

Fig. 8 Graphical representation of the AIM analysis of $(C_9H_{15}N_3)[CuCl_4(H_2O)]$: Red and Yellow dots indicate the position of the bond and new ring critical points, respectively

Fig. 9 (a) and (b) f^- and f^+ Fukui functions of $(C_9H_{15}N_3)^+$ respectively, the (c) Dual descriptor of the title compound.

Fig. 10 Different types of interactions between $(C_9H_{15}N_3)[CuCl_4(H_2O)]$, 4MQQ and 6GQO bacteria.

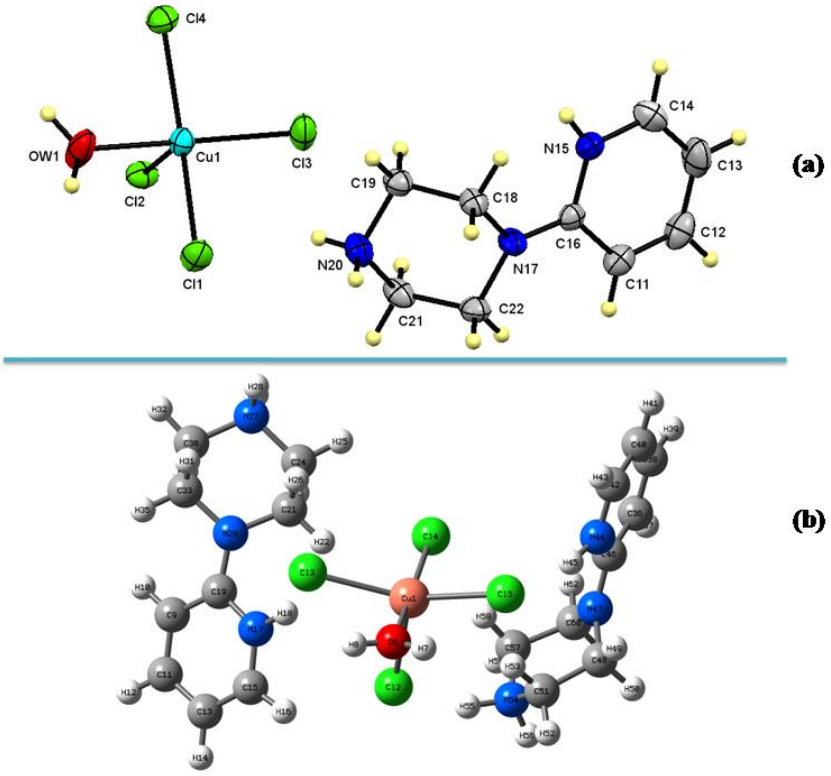

Figure 1

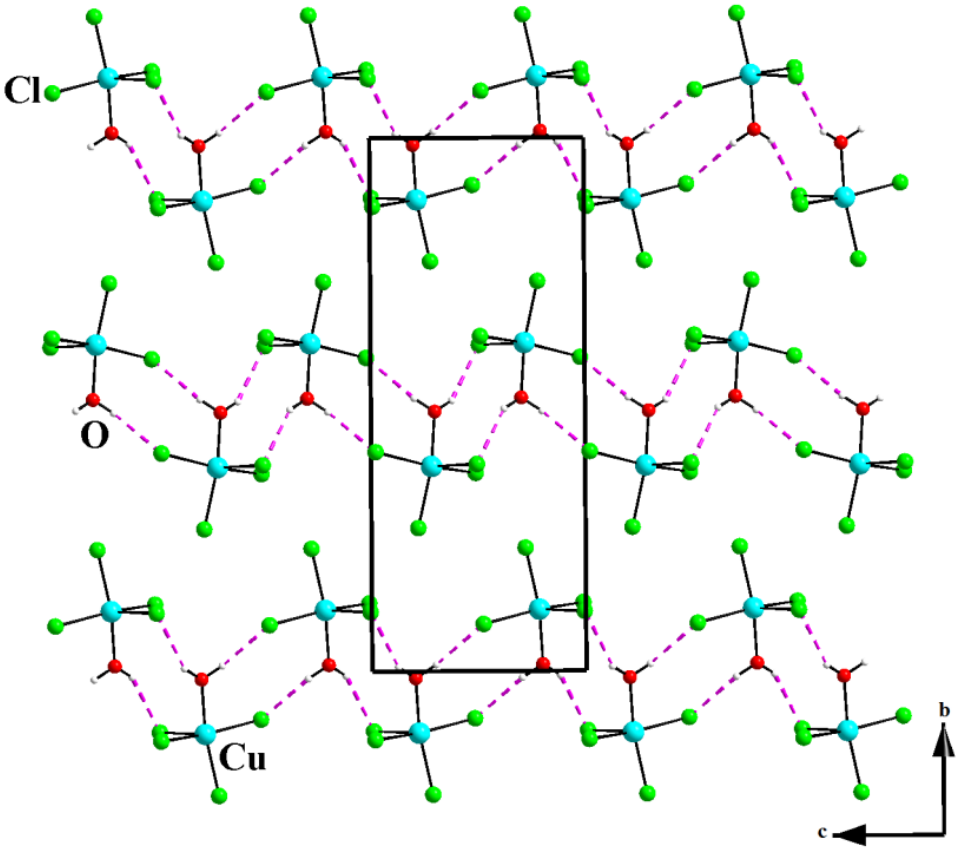

Figure 2

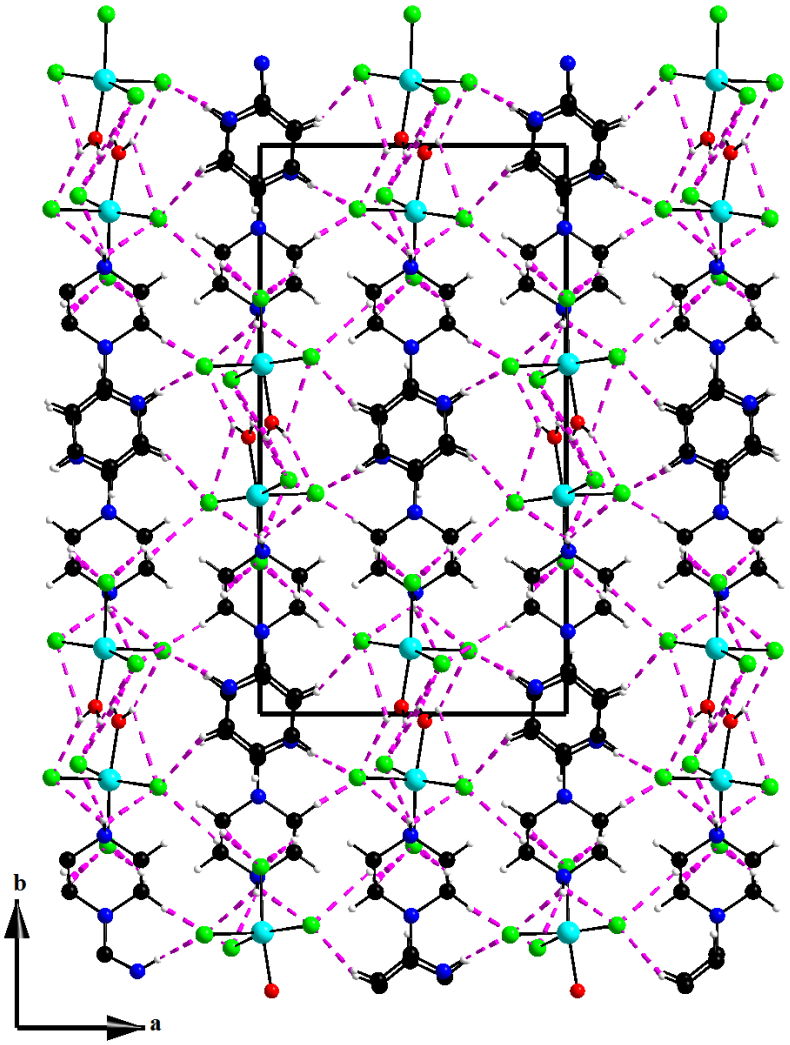

Figure 3

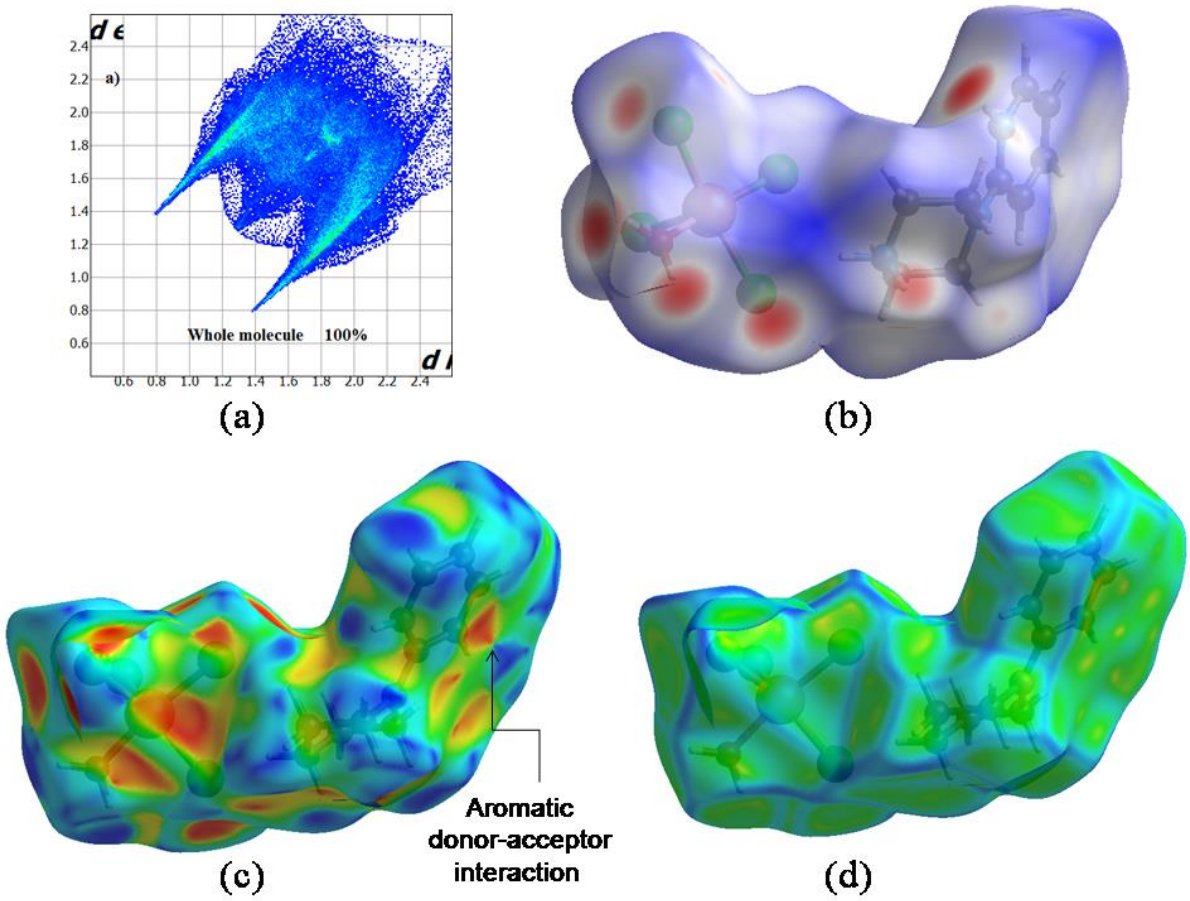
a)
Whole molecule 100%
(a)
(b)
Aromatic
donor-acceptor
interaction
(c)
(d)

Figure 4

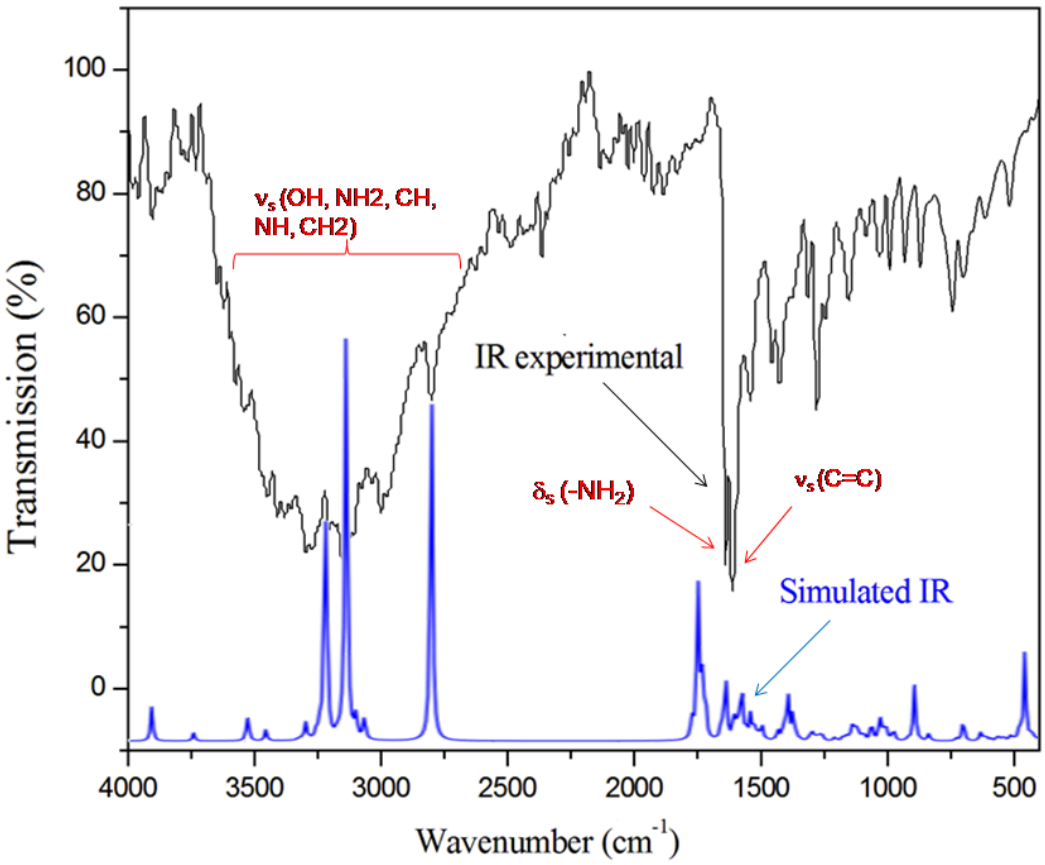
Transmission (%)
100
80
60
40
20
0
4000
3500
3000
2500
2000
1500
1000
500
Wavenumber (cm-1)
νs (OH, NH2, CH, NH, CH2)
IR experimental
δs (-NH2)
νs (C=C)
Simulated IR

Figure 5

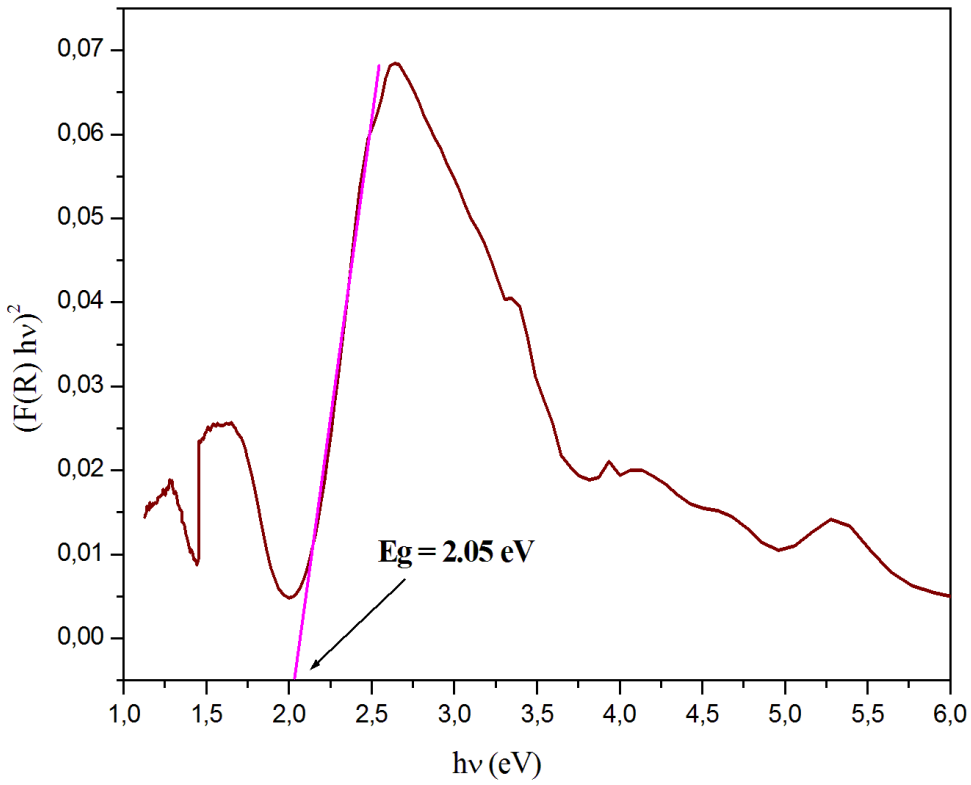

Figure 6

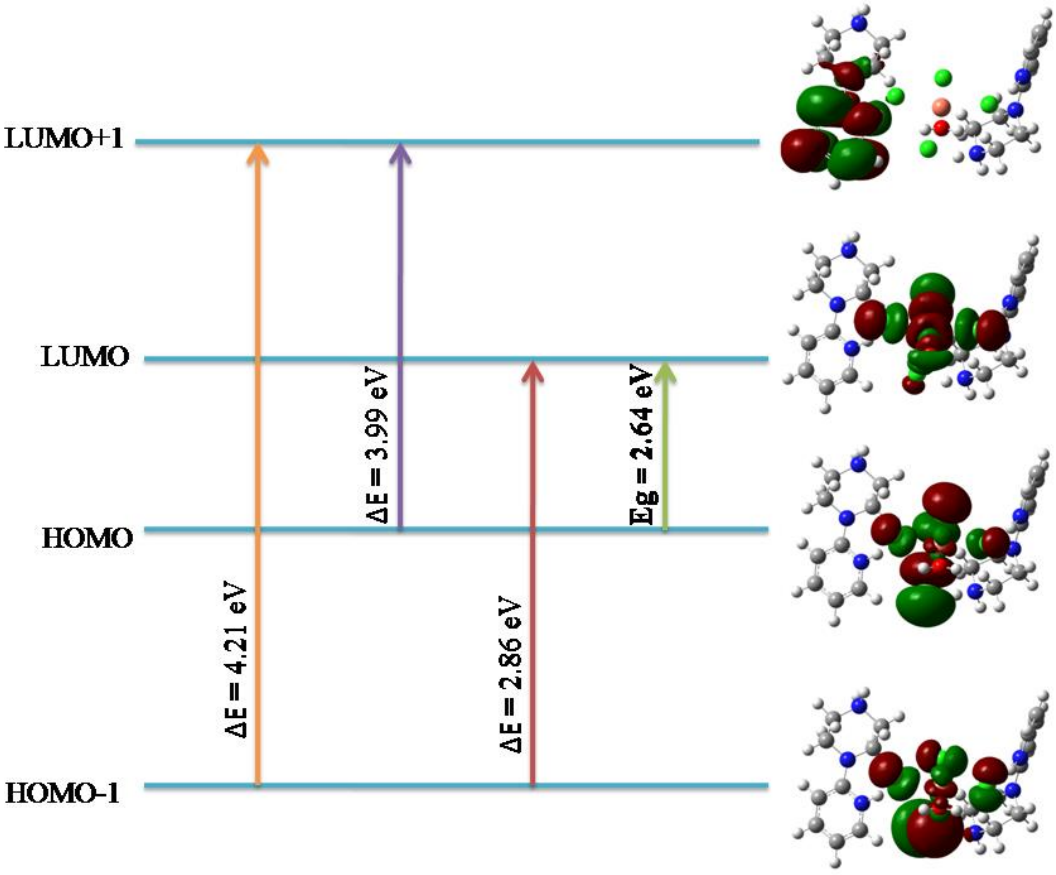

Figure 7

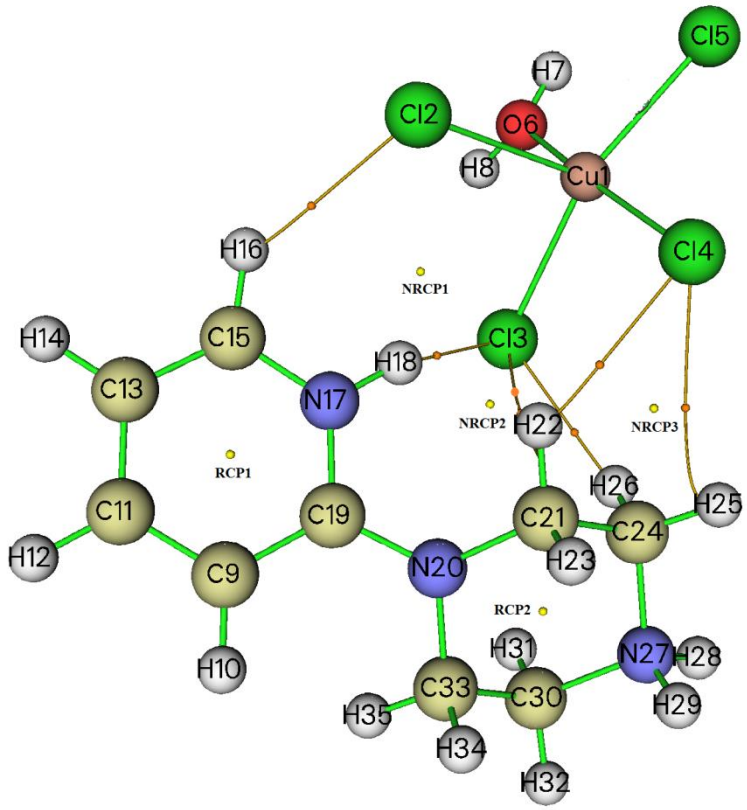

Figure 8

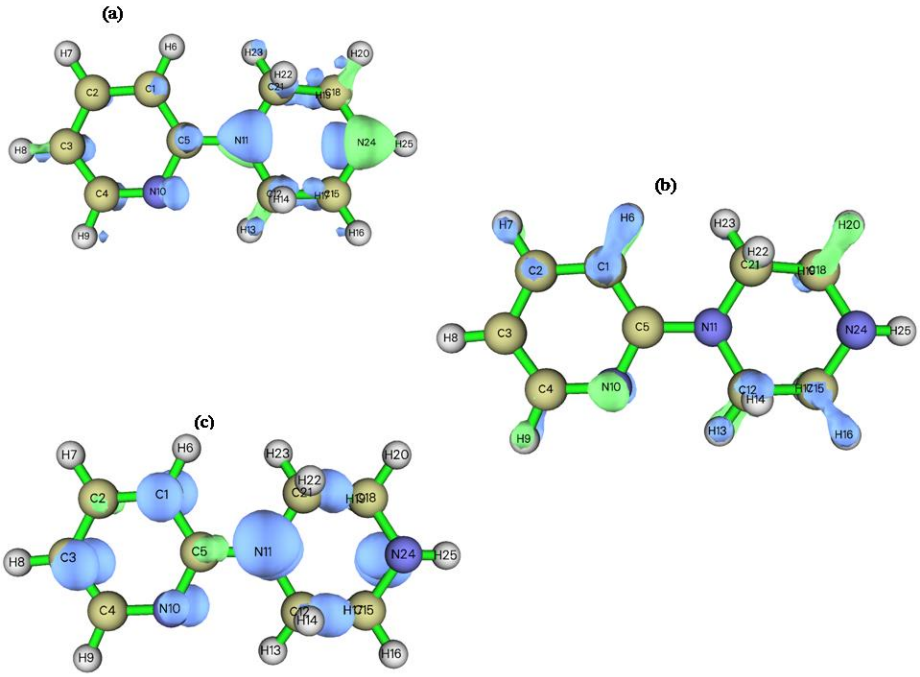

Figure 9

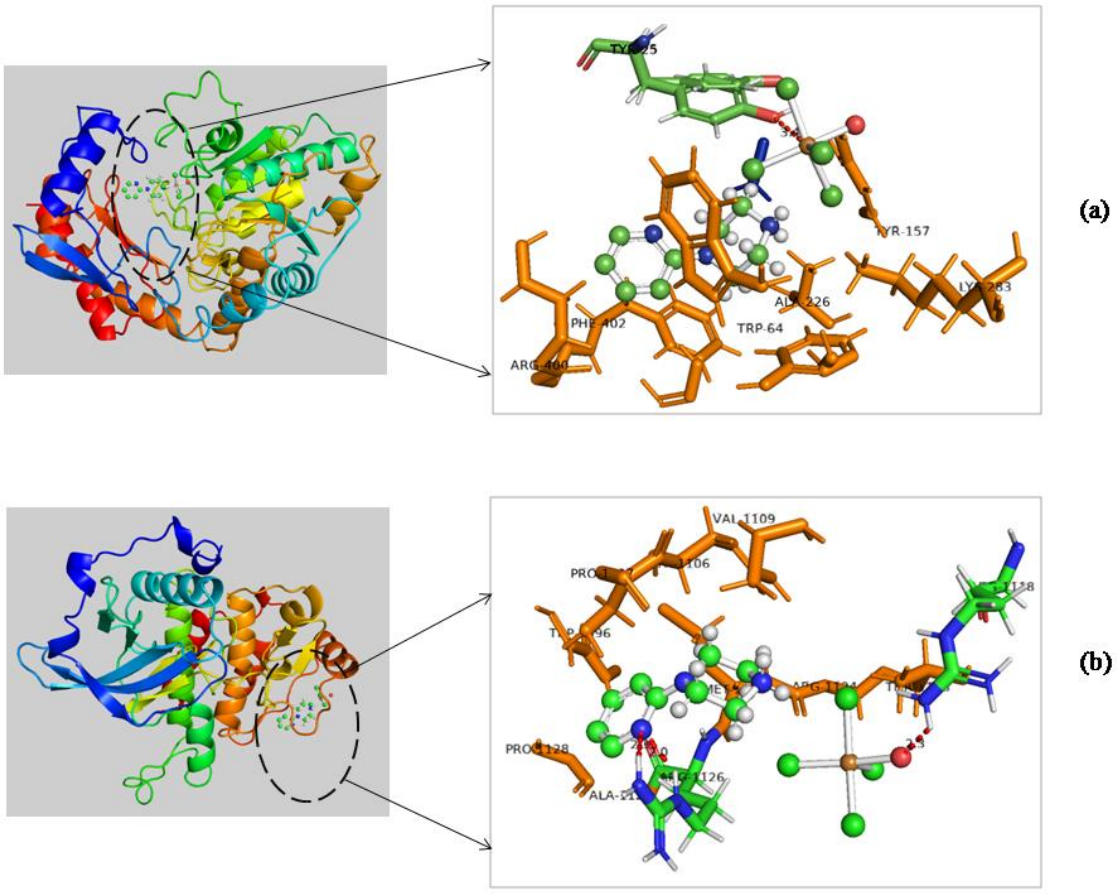

Figure 10

Graphical Abstract

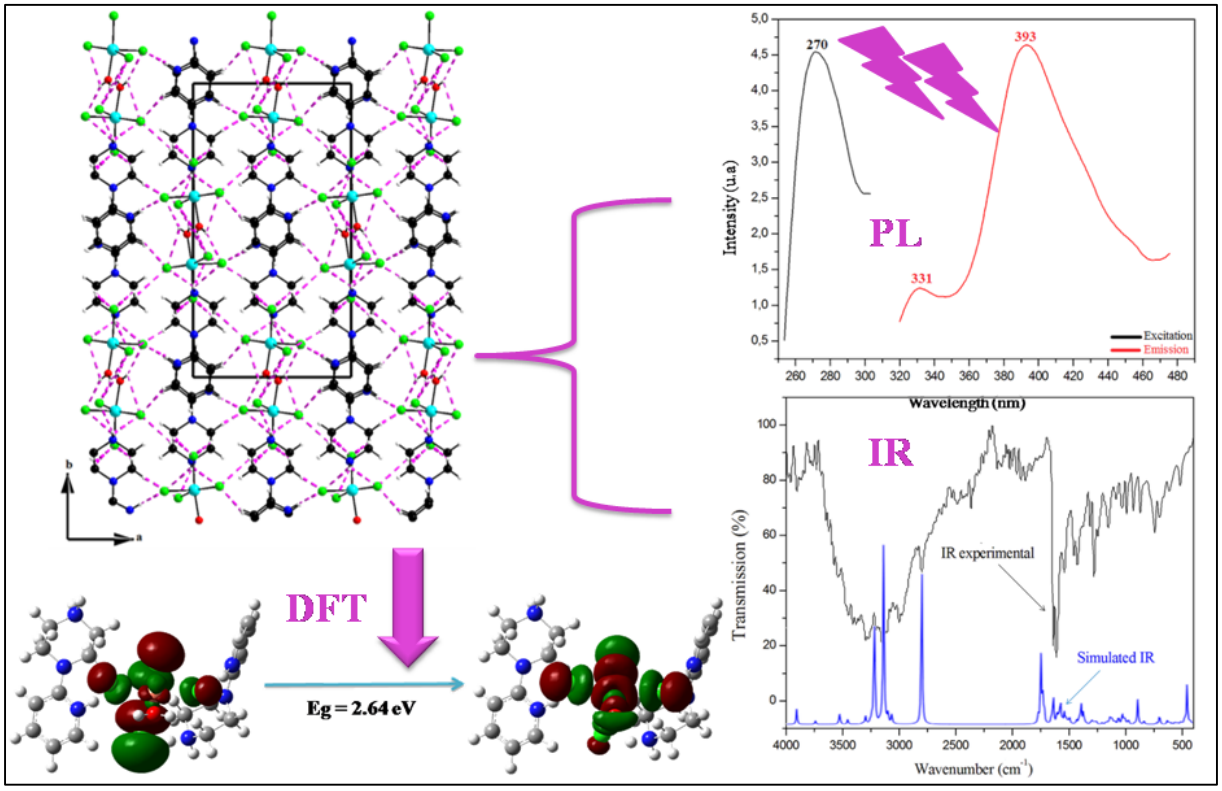

X-Ray diffraction, IR spectrum, optical properties, AIM, NBO, RDG, HS, Fukui function, biological and molecular docking analysis of a novel hybrid compound ($C_9H_{15}N_3$)[$CuCl_4(H_2O)$]

Afef Gannouni[a], Wiem Tahri[b], Thierry Roisnel[c], Kefi Riadh[a]

[a]*Laboratoire de Chimie des Matériaux, Faculté des Sciences de Bizerte, 7021 Zarzouna, Tunisie.*
[b]*Laboratory of Biochemistry and Molecular Biology, Faculty of Sciences, Risks Related to Environmental Stress, Struggle and Prevention (UR17ES20), University of Carthage, Te Ministry of Higher Education and Scientifc Research, Zarzouna, 7003 Bizerte, Tunisia.*
[c] *Univ Rennes, CNRS, ISCR (Institut des Sciences Chimiques de Rennes) – UMR 6226, F-35000 Rennes, France.*

Table captions

Table 1 Crystallographic data and structure refinement parameters of $(C_9H_{15}N_3)[CuCl_4(H_2O)]$

Table 2 Hydrogen bonding parameters (Å, °) for $(C_9H_{15}N_3)[CuCl_4(H_2O)]$

Table 3 Selected bond lengths (Å) and bond angles (°) in anions $[CuCl_4(H_2O)]^{-2}$

Table 4 Selected bond lengths (Å) and bond angles (°) in cations $[C_9H_{15}N_3]^{2+}$

Table 5 Hirshfeld contact surfaces, derived random contacts and enrichment ratios of $(C_9H_{15}N_3)[CuCl_4(H_2O)]$

Table 6 Main calculated optical transitions for the cluster with oscillator strength and major contribution. A comparison between the theoretical and experimental absorption features of $(C_9H_{15}N_3)[CuCl_4(H_2O)]$.

Table 7 The calculated HOMO-LUMO energy values, gap energy, chemical potential, chemical hardness, electrophilicity index, softness and electronegativity of $(C_9H_{15}N_3)[CuCl_4(H_2O)]$.

Table 8 Topological parameters (distance, electron density, Laplacien, Potential energy density, interaction energy, ellipticity and eta index) of $(C_9H_{15}N_3)[CuCl_4(H_2O)]$.

Table 9 Molecular docking results of binding energies in $kcal.mol^{-1}$ via Igemdock program.

Table 1

Crystal data	
Chemical formula	$(C_9H_{15}N_3)[CuCl_4\,(H_2O)]$
Formula weight (g/mol)	388.59
Crystal system	monoclinic
Space group	$P2_1/n$
a, b, c (Å)	10.2986 (8), 19.1385 (13), 7.6984 (5)
β (°)	90.134(4)
Volume V ($Å^3$)	1517.37(19)
Z	4
Crystal size (mm^3)	0.510 x 0.440 x 0.190
Radiation (Wavelength (Å))	0.71073
F (000)	788
Density (calculated), (mg/m^3)	1.701
Diffractmeter	APEX-II Kappa-CCD
Theta range for data collection (°)	2.8719 – 27.1497
Reflections collected	7420
Index ranges	h = -13/9; k = -15/24; l = -9/9
No. of measured, independent &	3444, 3388
observed [I > 2s(I)] reflections	3004
Absorption coefficient/[mm^{-1}]	2.135
Abs.correction	Multi-scan
Max and min. transmission	0.667 and 0,494
Goodness-of-fit on F^2	1.044
Final R indices [I > 2s (I)]	0,024
R indices [all data]	0,052
Largest diff. peak and hole [e $Å^3$]	-0.352, 0.561

Table 2

D – H ⋯ A	D – H (Å)	H⋯A (Å)	D⋯A (Å)	D – H⋯A (°)
OW1 – H1B⋯Cl2	0.89(2)	2.43(3)	3.231(3)	151(3)
OW1 – H1B⋯Cl1	0.90	2.36(3)	3.179(3)	151(3)
C14 – H14 ⋯ Cl4	0.93	2.59	3.460(4)	156.6
N15 – H15 ⋯ Cl2	0.82(3)	2.34(4)	3.093(3)	153(4)
C19 – H19B⋯Cl3	0.97	2.83	3.533(4)	129.7
N20 – H20A⋯Cl1	0.82(3)	2.44(4)	3.212(3)	157(3)
N20 – H20B⋯Cl2	0.89(3)	2.71(4)	3.386(3)	133(3)
N20 – H20B⋯C14	0.89(3)	2.57(4)	3.254(3)	134(3)
C21 – H21A⋯Cl4	0.97	2.80	3.480(3)	129.3

Table 3

$[CuCl_4(H_2O)]^{2-}$

Band	**Experimental**	**theoretical**	**Band**	**Experimental**	**theoretical**
Distances					
Cu1 - OW1	1.996(2)	1.989	Cu1 - Cl3	2.2650(8)	2.645
Cu1 - Cl1	2.3193(9)	2.460	Cu1 - Cl4	2.2875(9)	2.453

Cu1 - Cl2	2.5494(9)	2.336			
Angles					
Cl3 - Cu1 - Cl4	93.51(3)	96.11	OW1 - Cu1 - Cl4	87.36(8)	82.82
OW1 - Cu1 - Cl1	84.22(8)	81.31	Cl3 - Cu1 - Cl1	91.32(3)	114.01
Cl4 - Cu1 - Cl1	160.49(4)	146.86	OW1 - Cu1 - Cl2	92.95(9)	172.11
Cl3 - Cu1 - Cl2	98.44(3)	93.17	Cl4 - Cu1 - Cl2	96.23(3)	96.80
Cl1 - Cu1 - Cl2	101.75(3)	95.05	OW1 - Cu1 - Cl3	168.40(9)	94.70

Table 4

$[C_9H_{15}N_3]^{2+}$

Angles	**Experimental**	**theoretical**	**Angles**	**Experimental**	**theoretical**
Distances					
C11 - C12	1.355(5)	1.4	N15 - C16	1.351(4)	1.372
C11 - C16	1.420(4)	1.416	C16 - N17	1.338(4)	1.388
C12 - C13	1.388(5)	1.415	N17 - C22	1.463(4)	1.471
N17 - C18	1.464(4)	1.484	N20 - C21	1.497(4)	1.533
C13 - C14	1.344(5)	1.389	C19 - N20	1.485(4)	1.544
C18 - C19	1.502(4)	1.531	C21 - C22	1.501(4)	1.540
Angles					
C12 - C11 - C16	120.4(3)	119.72	N17 - C16 - N15	119.3(3)	118.09
C11 - C12 - C13	121.2(3)	120.63	N15 - C16 - C11	115.7(3)	117.62
C14 - C13 - C12	118.2(3)	118.35	N17 - C16 - C11	125.0(3)	124.29
C13 - C14 - N15	120.7(3)	119.98	C16 - N17 - C22	123.9(3)	121.42
C16 - N15 - C14	123.8(3)	123.62	C16 - N17 - C18	124.5(3)	122.75
C22 - N17 - C18	111.4(2)	113.89	N17 - C18 - C19	110.9(3)	111.56
N20 - C19 - C18	108.9(3)	109.67	C19 - N20 - C21	112.6(2)	111.39
N20 - C21 - C22	110.5(3)	110.16			

Table 5

Atome	H	Cl	C	N	O	Cu
Surface (S, %)	63.15	27.3	5.75	1.55	0.95	0.8
Contactes (C, %)	H	Cl	C	N	O	Cu
Cl	**54.1**	-	0.4	-	0.1	-
H	**31.5**	-	**4.2**	1.6	1.8	1.6
C	-	-	**2.7**	1.5	-	-
Contactes imaginaires (R, %)	H	Cl	C	N	O	Cu
H	39.88	-	-	1.96	1.2	1.01
Cl	34.48	-	0.18	-	0.52	-
C	7.26	-	0.073	0.18	-	-
Enrichissement (E)	H	Cl	C	N	O	Cu
$\mathbf{E_H}$…	0.79	1.57	0.58	0.82	1.5	1.58
$\mathbf{E_C}$…	-	2.22	**36.99**	**8.33**	-	-
$\mathbf{E_{Cl}}$…	-	-	-	-	0.19	-

Table 6

Experimental	Theoretical			
Wavelength (nm)	**Wavelength (nm)**	**Transition (nm)**	**Oscillator strength**	**Nature (%)**
-	472.32	TCML	0.0005	H → L (100 %)
350	433.51	$\pi\rightarrow\pi^*$, $n\rightarrow\pi^*$	0.0	H → L+1 (100%)
300	414.01	TCML	0.0014	H-1 → L (100%)
270	386.59	TCanion-cation	0.0	H-1 → L+1 (97%)

Table 7

Parameters	**Values (eV)**
E_{HOMO}	-10.909
E_{LUMO}	-8.27
Energy band gap $\lvert E_{HOMO}-E_{LUMO}\rvert$	2.64
Chemical hardness $\eta = \frac{(I-A)}{2}$	1.3195
Chemical potential for the molecule $\mu = \frac{-(I+A)}{2}$	-9.5895
The softness $S = \frac{1}{2\eta}$	0.3789
Electrophilicity index of the molecule $W = \frac{\mu^2}{2\eta}$	34.8459
Electonegativity $\chi = \frac{(I+A)}{2}$	9.5895

Table 8

	D (Å)	**ρ(r) (a.u)**	**$\nabla^2\rho$(r)(a.u)**	**V(r) (a.u)**	**Eint (kcal.mol^{-1})**	**(ε)**	**(ζ)**
H26···Cl3	2.449570	0.2061250	-0.2943204	-0.282949140	-69.5697	0.0542	0.9691
H18···Cl3	2.163903	0.2641818	-0.8473619	-0.293499740	-88.8643	0.0445	1.3802
H22···Cl3	3.076449	0.3208060	-0.148 10^{+1}	-0.48409656	-107.6828	0.0216	1.0237
H22···Cl4	2.732576	0.2724941	-0.9377254	-0.30991442	-91.6268	0.0355	1.4309
H25···Cl4	3.078938	0.2295457	-0.4688915	-0.23258382	-77.3533	0.0565	1.2361
H16···Cl2	2.644145	0.2691843	-0.9100786	-0.30486604	-90.5268	0.0092	1.4288
RCP1	--	0.533610^{-2}	0.1731 10^{-1}	-0.2583 10^{-2}	--	-1.6473	0.2206
RCP2	--	0.2892867	-0.772659	-0.3859261	--	0.1379	2.2095
NRCP1	--	0.2701671	-0.1133972	-0.372581408	--	0.0004	1.1912
NRCP2	--	0.3203314	-0.148 10^{+1}	-0.4833705	--	0.0216	1.0236
NRCP3	--	0.2191 10^{-1}	0.16504729	-0.3042810^{-1}	--	-1.2207	0.1921

D (Å): Distance; ρ(r) (a.u.): Density of electrons; ∇^2 ρ(r) (a.u): Laplacian of electron density; V(r) (a.u): Potential energy density; (Eint) (kJ.mol^{-1}): Interaction energy; (ε): Ellipticity; (ζ): Eta index, NRCP: new ring critical point.

Table 9

Ligand	receptor	Total energy	VDW	H-Bond	Electronic	AverConPair
$(C_9H_{15}N_3)[CuCl_4(H_2O)]$	4MQQ	-96.5416	-96.7778	0	0.236219	24.5357
	6GQO	-96.4865	-88.6652	-8.3075	0.486269	23.2143
	6GQP	-88.4408	-85.4328	-3.5	0.492034	20.4286
	3TFT	-86.5265	-82.6401	-3.5	-0.38639	22.5714
	3G60	-83.792	-81.292	-2.5	0	19.6786
	3PWH	-82.0833	-78.7185	-3.6376	0.2727	19.9643
	3W37	-81.627	-77.6727	-3.3812	-0.57313	19.7857
	1Y6B	-74.0556	-74.0556	0	0	17.3929

Supporting Material to

X-Ray diffraction, IR spectrum, optical properties, AIM, NBO, RDG, HS, Fukui function, biological and molecular docking analysis of a novel hybrid compound ($C_9H_{15}N_3$)[$CuCl_4(H_2O)$]

Afef Gannouni[a], Wiem Tahri[b], Thierry Roisnel[c], Kefi Riadh[a]

[a] *Laboratoire de Chimie des Matériaux, Faculté des Sciences de Bizerte, 7021 Zarzouna, Tunisie.*
[b] *Laboratory of Biochemistry and Molecular Biology, Faculty of Sciences, Risks Related to Environmental Stress, Struggle and Prevention (UR17ES20), University of Carthage, Te Ministry of Higher Education and Scientifc Research, Zarzouna, 7003 Bizerte, Tunisia.*
[c] *Université Rennes, CNRS, ISCR (Institut des Sciences Chimiques de Rennes) – UMR 6226, F–35000 Rennes, France.*

Figure S - 1: The cristal photo of ($C_9H_{15}N_3$)[$CuCl_4(H_2O)$]

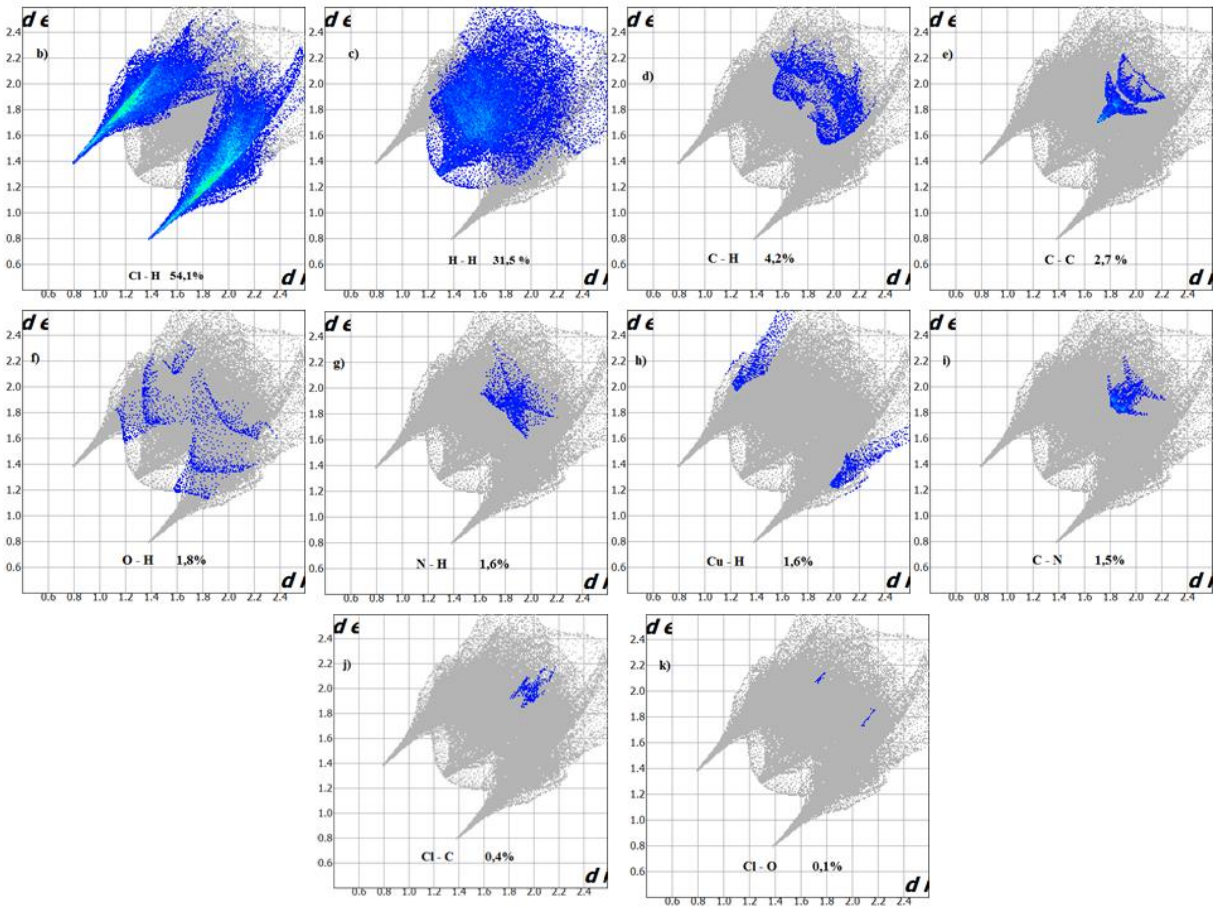

Figure S - 2 : The two-dimensional fingerprint plots for the title compound delineated into: (b) Cl…H, (b) H…H, (c) C…H, (d) C…C, (e) O…H, (f) N…H, (g) Cu…H, (h) C…N, (i) Cl…H, (j) Cl…C and (k) Cl…O

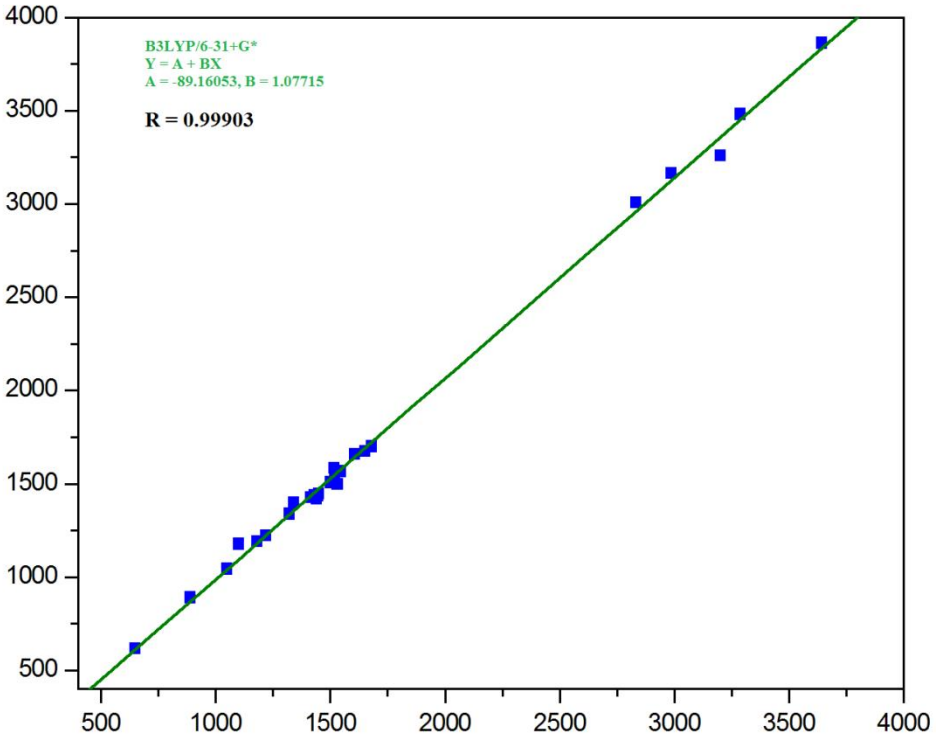

Figure S - 3 : Correlation graph between the experimental and calculated wave numbers (cm^{-1}) of $(C_9H_{15}N_3)[CuCl_4(H_2O)]$

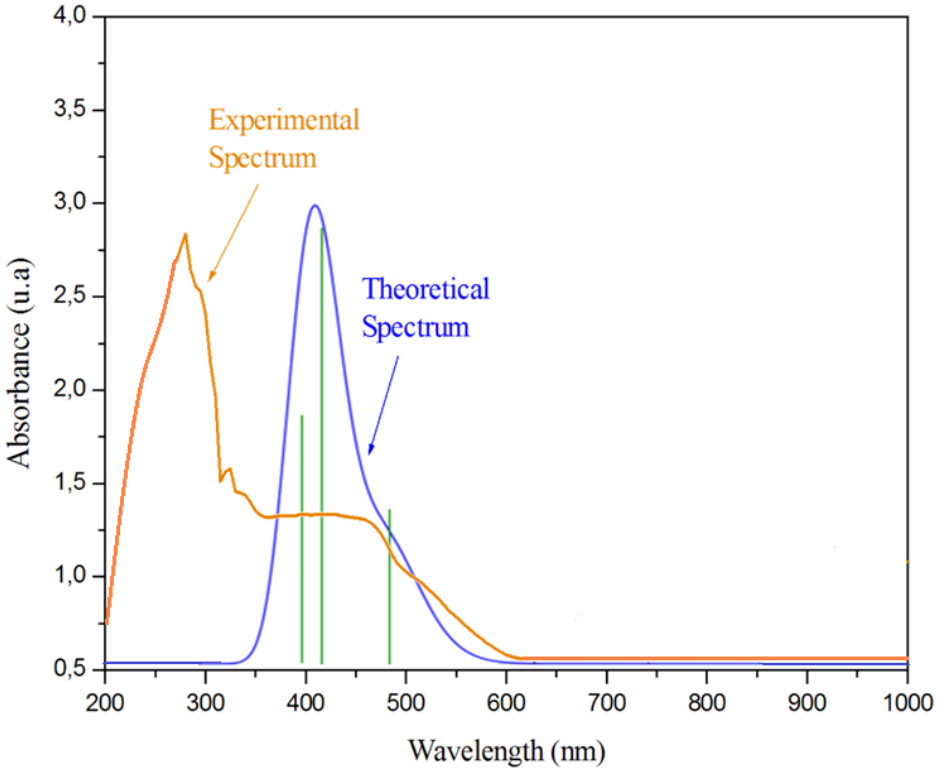

Figure S - 4 : Correlation graph between the experimental and calculated wavelength (nm) of $(C_9H_{15}N_3)[CuCl_4(H_2O)]$

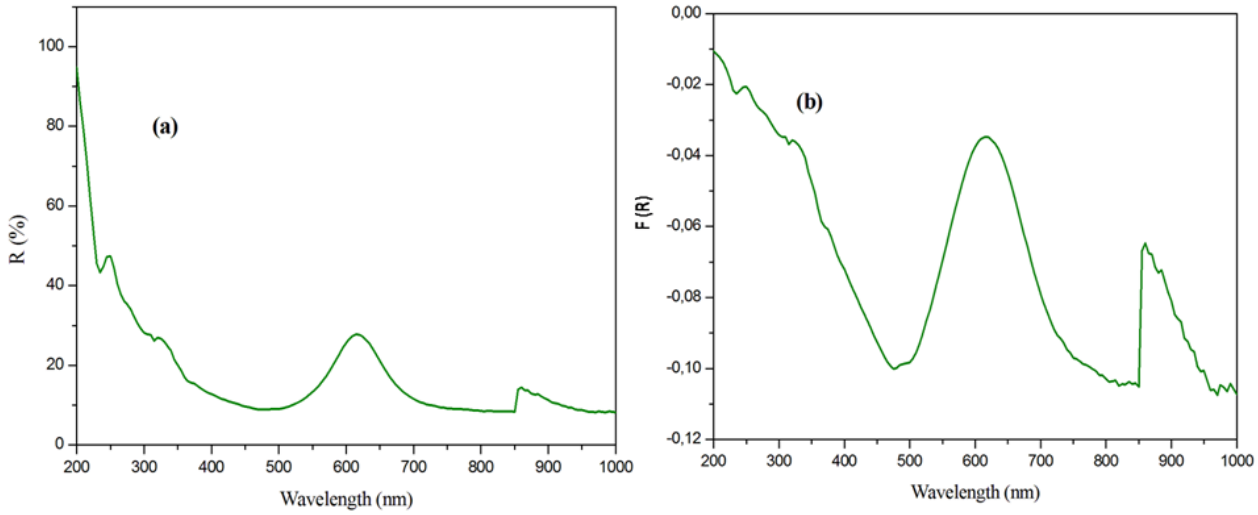

Figure S - 5 : (a): The diffuse reflectance spectra and (b): the Kubelka-Munk absorption spectra of $(C_9H_{15}N_3)[CuCl_4(H_2O)]$

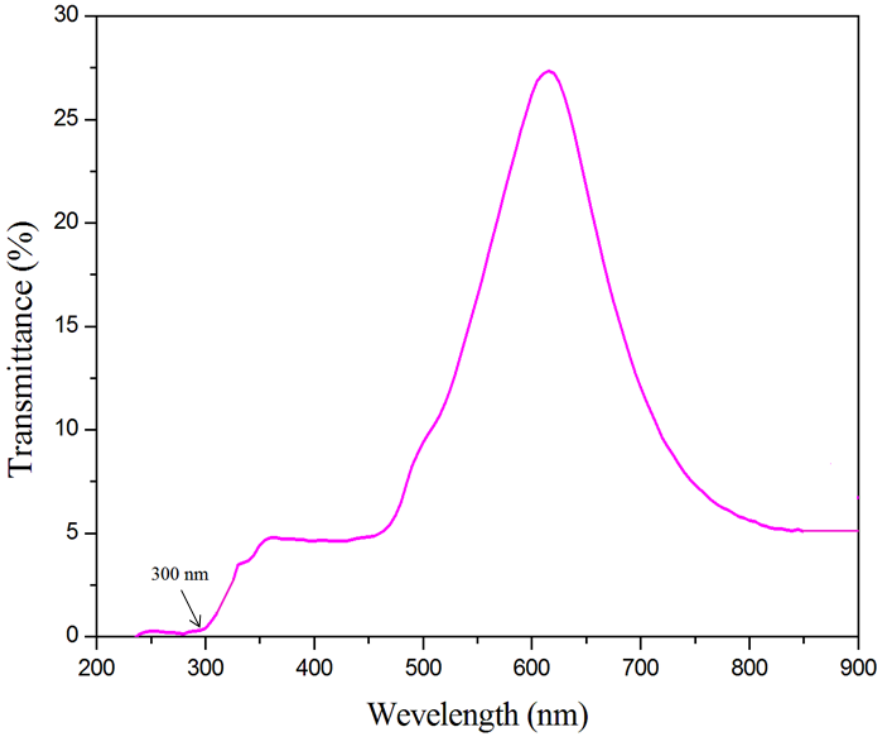

Figure S - 6 : Optical transmittance spectrum of $(C_9H_{15}N_3)[CuCl_4(H_2O)]$

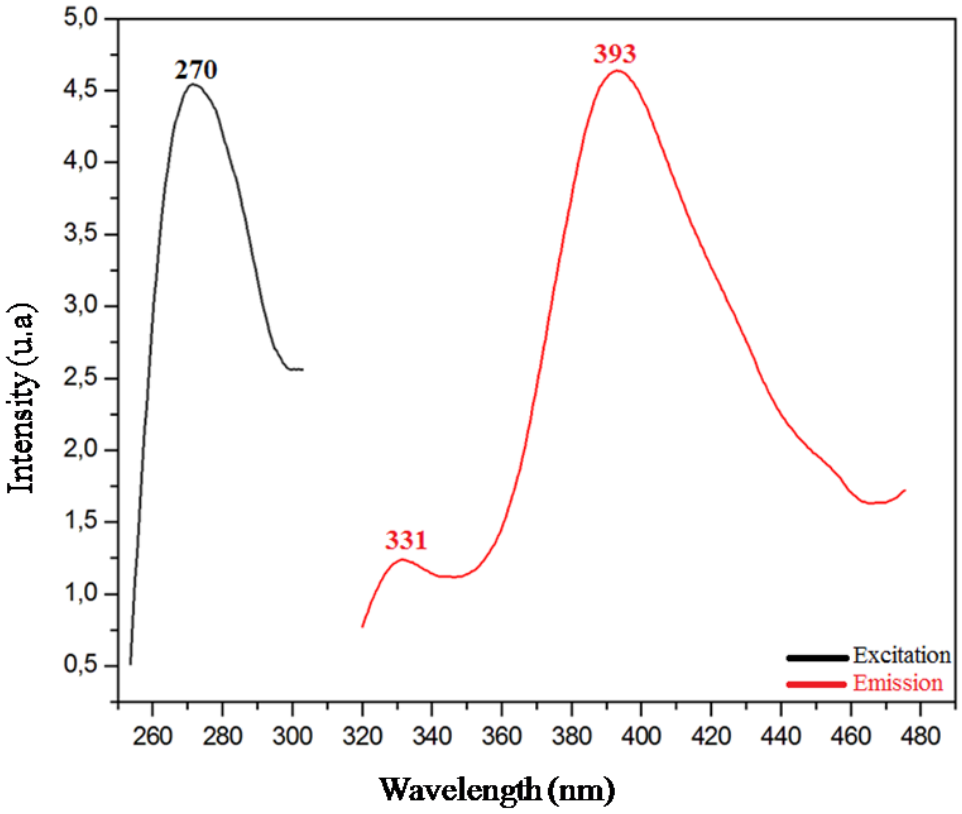

Figure S - 7 : The emission spectra of $(C_9H_{15}N_3)[CuCl_4(H_2O)]$

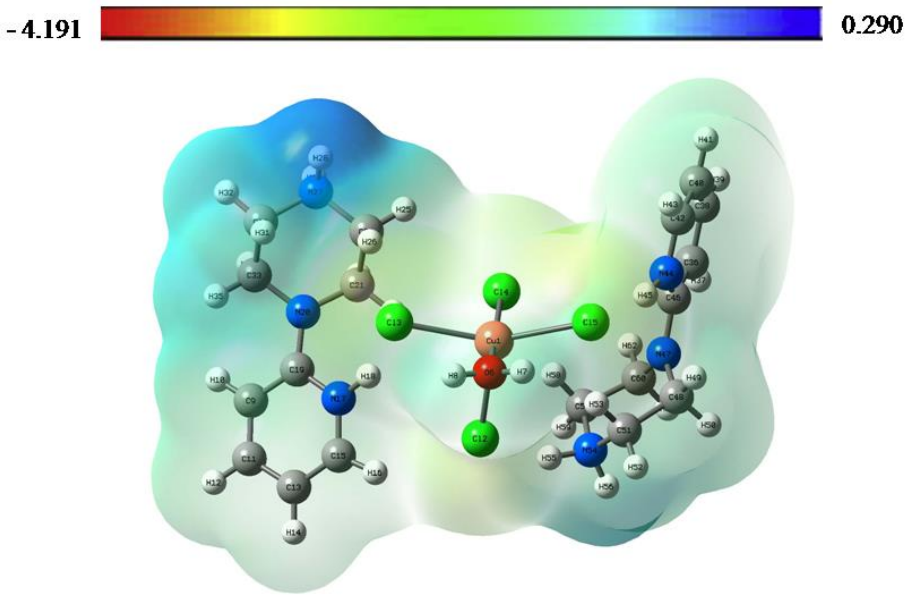

Figure S - 8 : Molecular electrostatic potential surface (between -4.191 and 0.290) of $(C_9H_{15}N_3)[CuCl_4(H_2O)]$

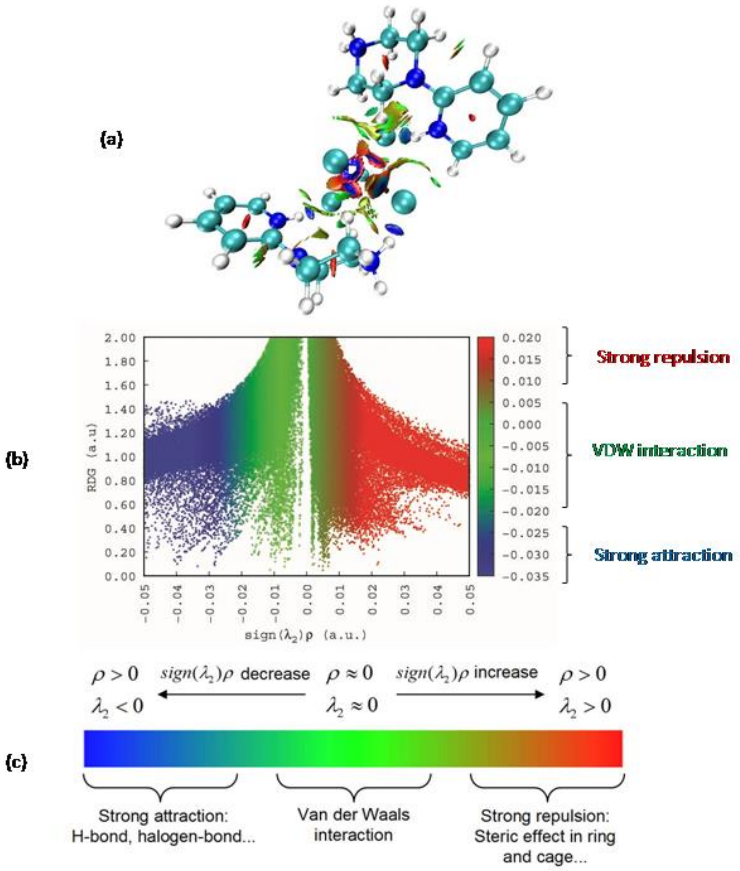

Figure S - 9 : Representation of different types of interactions in the monomer (a). Graph of the reduced density gradient vs. sign ($\lambda 2$) ρ of ($C_9H_{15}N_3$)[$CuCl_4(H_2O)$] (b). Color code for different regions of interactions (c).

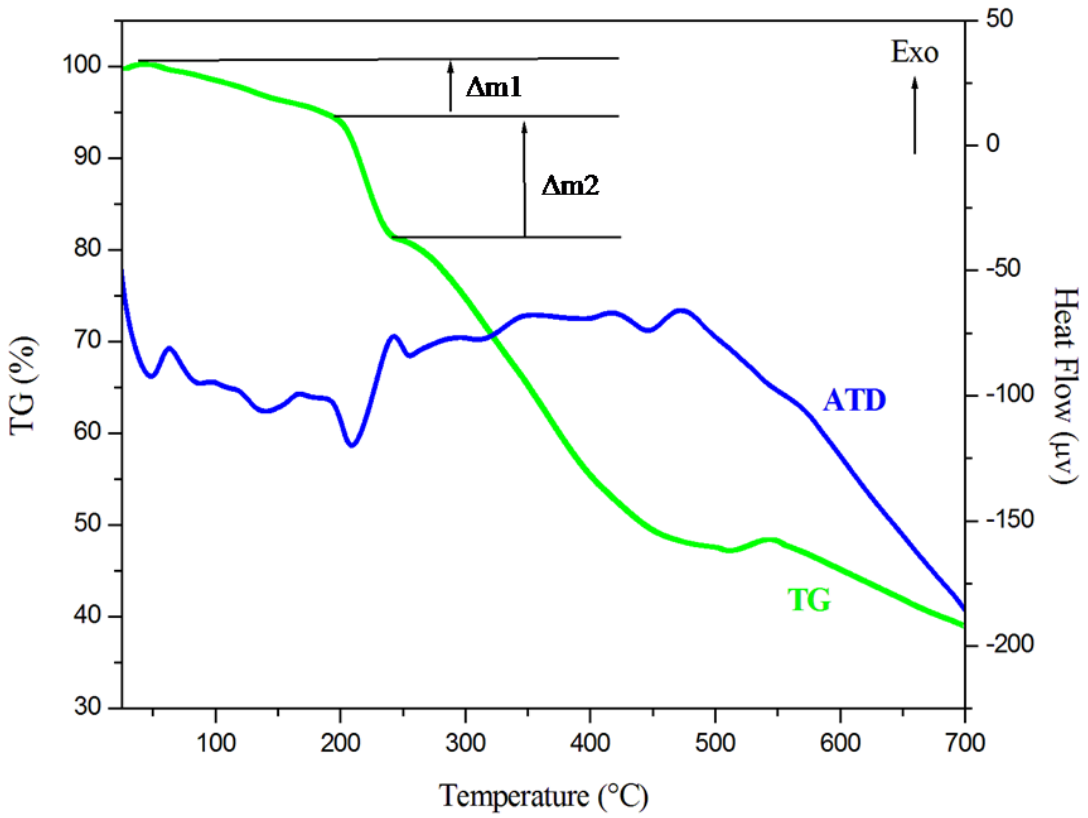

Figure S - 10 : Simultaneous curves of thermogravemetric analysis and differential thermal analysis of $(C_9H_{15}N_3)[CuCl_4(H_2O)]$.

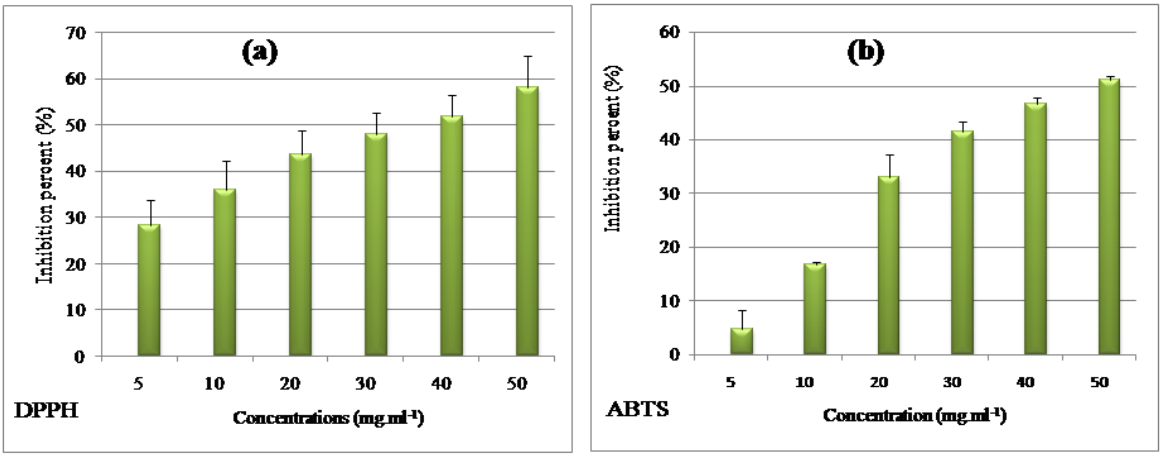

Figure S - 11 : Scavenging activity of $(C_9H_{15}N_3)[CuCl_4(H_2O)]$ in both (a) $DPPH^{\bullet+}$ and (b) $ABTS^{\bullet+}$ test. The data are reported as mean ± standard deviation

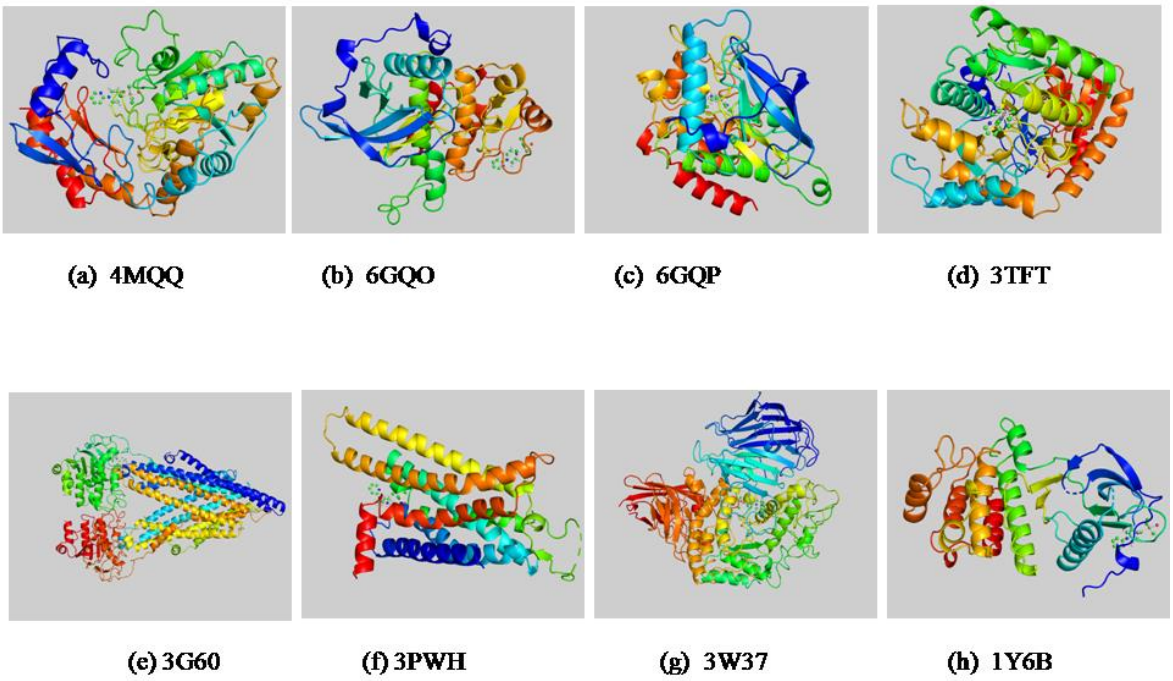

Figure S - 12: The best docked poses of 2PPCU compound with eight protein: (a) 4MQQ, (b) 6GQO, (c) 6GQP, (d) 3TFT, (e) 3G60, (f) 3PWH, (g) 3W37, (h) 1Y6B

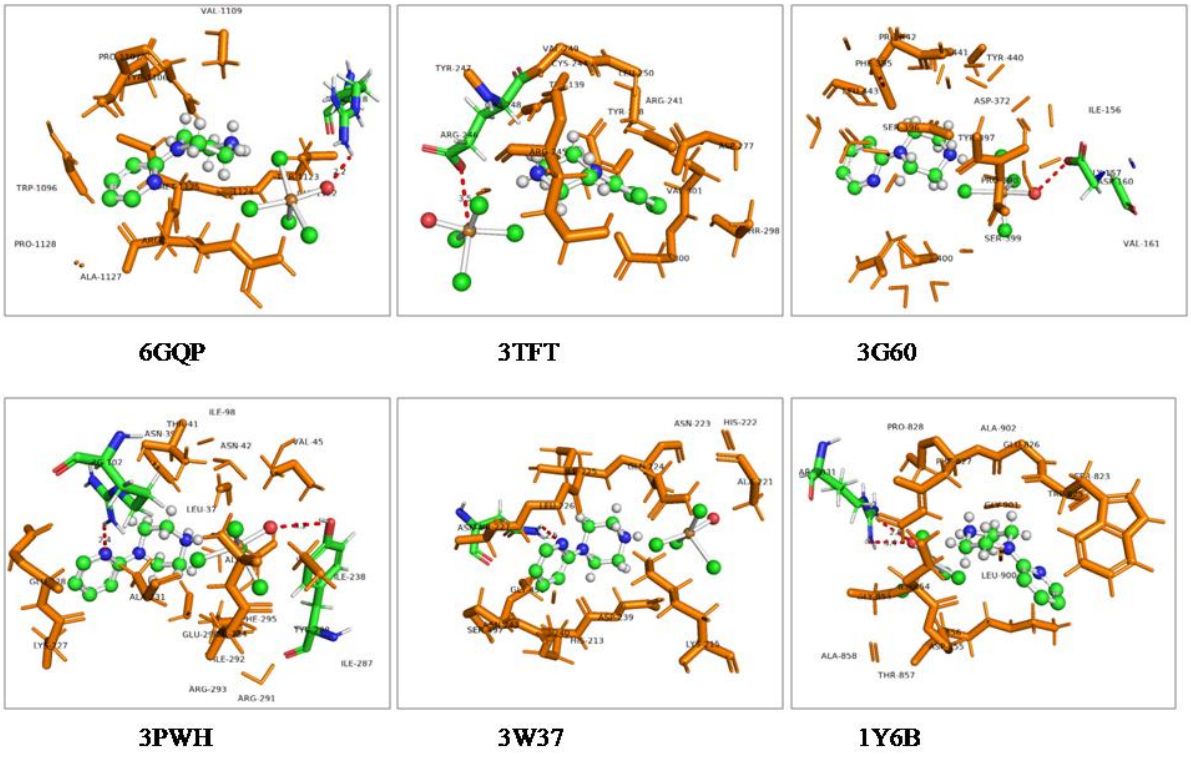

Figure S - 13 : Different types of interactions between $(C_9H_{15}N_3)[CuCl_4(H_2O)]$ and 6GQP, 3TFT, 3G60, 3PWH, 3W37, 1Y6B

Table S – 1: Assignments of IR vibrational modes in $(C_9H_{15}N_3)[CuCl_4(H_2O)]$

Frequenccy (cm^{-1})		**Attribution**
IR Experimental	**IR Theoretical**	
3642-3000	3695, 3863	**ν_s (OH)**
3288-3268	3481, 3406	**ν_s (-NH2)**
3200-3150	3260, 3235, 3247 3235, 3274	**ν_s (CH)**
2987	3164	**ν_s (-NH)**
2832-2800	3172, 3164, 3193, 3190 3193, 3190, 3158, 3112 3013, 3007	**ν_s (CH2)**
1627	1701, 1454, 1338, 1270	**δ_s (-NH_2)**
1607	1674, 1659, 1128	**ν_s (C=C)**
1531	1674, 1659, 1499	**δ_s (-NH)**
1450	1674, 787, 386, 320	**δ_s (CNC)**
1414-900	1583, 1128, 1082, 899 1068, 1019, 1062, 941	**ν_s (C-C)**
1515-1220	1583, 1428, 1421, 1223 1499, 1128, 1331, 1297 1499, 1439, 1331 1318 1338, 1207, 1207	**δ_s (C-C)**
1547	1566	**δ_s (H_2O)**
1520-1510	1533, 1516, 1522	**δ_s (CH)**
1500	1508	**δ_{as} (CH)**
1450	1467, 1270, 738, 899 1190, 1062, 1082, 738	**ν_s (C-N)**
1445-1200	1467, 1297, 1207	**δ_s (CN)**
1438	1454, 1421, 1418 949, 898	**τ_s(HNCC)**
1430-750	1439, 1032, 1032, 386	**τ_s(HCNC)**
1340	1399	**τ_{as}(HCCN)**
1320	1338	**τ_s(HCCN)**
1220	1223	**δ_{as} (CC)**
1180	1190, 751	**τ_s(CCNC)**
1100-500	1177, 899, 505, 469 787, 613, 642, 642 286, 218, 162	**δ_s (NCC)**
1090-805	1056, 1053, 751, 811 1044, 1019, 949, 898	**τ_s(HCCC)**
1048-723	1044, 1019, 642 1019, 738	**δ_s (CCC)**
890	891	**τ_s(CNCC)**
650	891, 218	**γ_s(CCCN)**
--	616, 611	**δ_s(CuO)**
--	542, 414	**τ_s(CCCC)**
--	451	**δ_{as} (NCC)**
--	426	**ν_s (Cu-O)**

--	386	**τ_s(NCCN)**
--	368, 341	**t_s(HOCuCl)**
--	320, 218	**τ_s(CCCN)**
--	263, 257, 250, 174	**ν_s (Cu-Cl)**
--	194, 162, 128	
--	174, 153, 103	**γ_s(OClClCu)**
--	153, 146, 140, 95	
--	143, 129, 113, 90	**δ_s(OCuCl)**
--	143, 129, 113, 103	**δ_s(ClCuCl)**
--	83, 32	**τ_s(CNCN)**
--	77, 72, 40	**τ_s(CuClHN)**
--	77, 69, 43	**τ_s(CNHCl)**
--	43, 17, 5	**t_s(HClCuCl)**
--	32	**δ_{as} (Cu-Cl)**

Table S – 2: NBO results showing the formation of Lewis and non-Lewis orbitals in $(C_9H_{15}N_3)[CuCl_4(H_2O)]$

Bonde A-B	Occupancy	EDA(%)	EDB(%)	NBO	Orbital atomique (%)
σ O6-H7	0.99759	77.80	22 .20	0.8820(sp2.43) O6 0.4712 s H7	s(29.17%)p(70.83) s(100%)
σ O6-H8	0.99755	77.77	22.23	0.819(sp2.44) O6 0.4715 s H8	s(29.08%)p(70.92) s(100%)
σ C9-H10	0.98708	62.17	37.83	0.7885(sp2.30) C9 0.6151 s H10	s(30.34%)p(69.66%) s(100%)
π C9-C11	0.82653	56.24	43.76	0.7499(sp99.99) C9 0.6615(sp1) C11	s(0.02%)p(99.98%) s(0.01%)p(99.99%)
σ C9-C19	0.98594	48.89	51 .11	0.6992(sp1.97)C9 0.7149(sp1.59)C19	s(33.63%)p(66.37%) s(38.65%)p(61.35%)
σ C11-H12	0.98800	62 .82	37.18	0.7926(sp2.35) C11 0.6097 s H12	s(29.84%)p(70.16%) s(100%)
σ C11-C13	0.99059	50.25	49.75	0.7089(sp1.86) C11 0.7053(sp1.89) C13	s(34.91%)p(65.09%) s(34.59%)p(65.41%)
σ C13-H14	0.98770	62.98	37.02	0.7936(sp2.2) C13 0.6085 s H14	s(31.29%)p(68.71%) s(100%)
π C13-C15	0.82257	54.80	45.20	0.7403(sp1)C13 0.6723(sp99.99) C15	s(0 %)p(100%) s(0.02%)p(99.98%)
σ C15-H16	0.98726	63.72	36.28	0.7983(sp2.02) C15 0.6023s H16	s(33.15%)p(66.85%) s(100%)
σ C15-N17	0.99247	35.99	64.01	0.5999(sp2.53) C15 0.8001(sp1.82) N17	s(28.33%)p(71.67%) s(35.46%)p(64.54%)
σ N17-H18	0.99003	76.09	23.91	0.8723(sp2.43) N17 0.4890s H18	s(29.11%)p(70.89%) s(100%)
π N17-C19	0.90737	72.54	27.46	0.8517(sp99.99) N17 0.5240(sp1)C19	s(0.10%)p(99.90%) s(0.01%)p(99.99%)
σ C19-N20	0.99069	38.07	61.93	0.6170(sp2.16) C19 0.7869(sp1.76) N20	s(31.63%)p(68.37%) s(36.28%)p(63.72%)
σ N20-C21	0.98888	63.55	36.45	0.7972(sp2.19) N20	s(31.34%)p(68.66%)

				0.6037(sp3.38) C21	s(22.85%)p(77.15%)
σ N20-C33	0.99051	62.50	37.50	0.7906(sp2.22) N20	s(31.10%)p(68.90%)
				0.6124(sp3.22) C33	s(23.69%)p(97.31%)
σ C21-H22	0.98389	64.22	35.78	0.8014(sp2.87) C21	s(25.84%)p(74.16%)
				0.5981s H22	s(100%)
σ C21-H23	0.98935	61.48	38.52	0.7841(sp3.16) C21	s(24.05%)p(75.95%)
				0.6207 s H23	s(100%)
σ C21-C24	0.99076	49.58	50.42	0.7041(sp2.67) C21	s(27.27%)p(72.73%)
				0.7101 (sp2.46 C24	s(28.92%)p(71.08%)
σ C24-H25	0.98731	63.15	36.85	0.7947(sp2.88) C24	s(25.75%)p(74.25%)
				0.6071 s H25	s(100%)
σ C24-H26	0.98836	63.98	36.02	0.7999(sp2.74) C24	s(26.74%)p(73.26%)
				0.6002s H260	s(100%)
σ C24-N27	0.99501	32.04	67.96	0 .5660(sp4.38) C24	s(18.58%)p(81.42%)
				0.8244(sp2.57) N27	s(28.03%)p(71.97%)
σ N27-H28	0.99328	74.21	25.79	0 .8614(sp3.47) N27	s(22.36%)p(77.64%)
				0.5152s H28	s(100%)
σ N27-H29	0.99475	73.46	26.54	0.8571(sp3.52) N27	s(22.13%)p(77.87%)
				0.5152s H29	s(100%)
σ N27-C30	0.99505	66.48	33.52	0.8153(sp2.65) N27	s(27.40%)p(72.60%)
				0.5790(sp4.13) C30	s(19.50%)p(80.50%)
σ C30-H31	0.98959	62.86	37.14	0.7928(sp2.9) C30	s(25.67%)p(74.33%)
				0.6094s H31	s(100%)
σ C30-H32	0.98874	62.63	37.37	0.7914(sp2.93) C30	s(25.46%)p(74.54%)
				0.6113s H32	s(100%)
σ C30-C33	0.99013	50.66	49.34	0.7118(sp2.41) C30	s(29.34%)p(70.66%)
				0.7024(sp2.74) C33	s(26.77%)p(73.23%)
σ C33-H34	0.99021	61.66	38.34	0.7852(sp3.04) C33	s(24.74%)p(75.26%)
				0.6192s H34	s(100%)
σ C33-H35	0.98519	62.90	37.10	0.79321(sp3.03) C33	s(24.80%)p(75.20%)
				0.6091s H35	s(100%)
LP(1)-Cu1	0.99987	-	-	spd1.00	s(0%)p(0%)d(100%)
LP(2)-Cu1	0.99980	-	-	sp(0.66)d(99.99)	s(0.13)p(0.08)d(99.7
LP(3)-Cu1	0.99974	-	-	sp1d(99.99)	s(0)p(0.05)d(99.95)
LP(4)-Cu1	0.99931	-	-	sp1d(99.99)	s(0)p(0.01)d(99.99)
LP(5)-Cu1	0.99854	-	-	sp(0.03)d(99.99)	s(0.20)p(0.01)d(99.7
LP*(6)Cu1	0.18108	-	-	sp0.07d0	s(93.02)p(6.66)d0.32
LP*(7)Cu1	0.11518	-	-	sp(99.99)d(0.72)	s(0.08)p(99.86)d(0)
LP*(8)Cu1	0.09805	-	-	sp(21.28)d(0.03)	s(4.48)p(95.38)d(0.1
LP*(9)Cu1	0.09176	-	-	sp(47.83)d(0.08)	s(2.04)p(97.8)d(0.15
LP(1)-Cl2	0.99260	-	-	sp(0.97)	s(50.86%)p(49.14%)
LP(2)-Cl2	0.98804	-	-	sp(12.51)	s(7.4%)p(92.60%)
LP(3)-Cl2	0.93387	-	-	sp(3.75)	s(21.07%)p(78.93%)
LP(4)-Cl2	0.91972	-	-	sp(3.84)	s(20.67%)p(79.33%)
LP(1)-Cl3	0.99546	-	-	sp(0.83)	s(54.69%)p(45.31%)
LP(2)-Cl3	0.97946	-	-	sp(52.32)	s(1.88%)p(98.12%)
LP(3)-Cl3	0.95554	-	-	sp(45.21)	s(2.16%)p(97.84%)
LP(4)-Cl3	0.91127	-	-	sp(1.42)	s(41.27%)p(58.73%)
LP(1)-Cl4	0.99482	-	-	sp(0.75)	s(57.12%)p(42.88%)
LP(2)-Cl4	0.98230	-	-	sp(68.68)	s(1.44%)p(98.56%)

LP(3)-Cl4	0.97852	-	-	sp(1.00)	s(0.01%)p(99.99%)
LP(4)-Cl4	0.89802	-	-	sp(1.41)	s(41.43%)p(58.57%)
LP(1)-Cl5	0.99390	-	-	sp(1.07)	s(48.29%)p(51.71%)
LP(2)-Cl5	0.98171	-	-	sp(99.99)	s(0.62%)p(99.38%)
LP(3)-Cl5	0.94940	-	-	sp(4.73)	s(17.46%)p(82.54%)
LP(4)-Cl5	0.91088	-	-	sp(1.97)	s(33.63%)p(66.37%)
LP(1)-O6	0.99357	-	-	sp(69.45)	s(1.42)p(98.58%)
LP(2)-O6	0.95274	-	-	sp(1.48)	s(40.29%)p(59.71%)
LP(1)N20	0.87108	-	-	sp(76.08)	s(1.3%)p(98.70%)
RY*(1)Cu1	0.00168	-	-	sp(83.43)d(6.15)	s(1.10)p(92.10)d(6.7
RY*(1)-O6	0.00091	-	-	sp(5.65)	s(15.04%)p(84.96%)
RY*(1)-H7	0.00063	-	-	s	s(100%)
RY*(2)-C9	0.00282	-	-	sp(99.99)	s(0.06%)p(99.94%)
RY*(1)C11	0.00338	-	-	sp(72.81)	s(1.35%)p(98.65%)
RY*(1)N17	0.00204	-	-	sp(99.99)	s(0.13%)p(99.87%)
RY*(1)N20	0.00593	-	-	sp(42.90)	s(2.28%)p(97.72%)
RY*(1)N27	0.00106	-	-	sp(28.87)	s(3.35%)p(96.65%)

Table S – 3: Second order perturbation theory analysis of Fock matrix basis in NBO basis corresponding to the intra molecular bonds in $(C_9H_{15}N_3)[CuCl_4(H_2O)]$

Donor	**Acceptor**	**$E^{(2)}$ Kcal/mol**	**E(j)-E(i) (a.u)**	**F(i,j) (a.u)**
LP(3)-Cl2	**LP*(9)-Cu(1)**	4.07	0.47	0.056
LP(4)-Cl2	**LP*(6)-Cu(1)**	15.54	0.36	0.100
LP(4)-Cl2	**LP*(9)-Cu(1)**	13.99	0.45	0.101
LP(3)-Cl3	**N17-H18**	8.53	0.64	0.093
O6-H8	**LP*(8)-Cu(1)**	5.88	1.02	0.103
LP(2)-O6	**LP*(6)-Cu(1)**	6.23	0.63	0.085
LP(2)-O6	**LP*(8)-Cu(1)**	26.15	0.82	0.190
C9-C11	**C13-C15**	6.97	0.29	0.059
C9-C11	**N17-C19**	21.48	0.20	0.089
C13-C15	**N17-C19**	6.71	0.20	0.049
C15-H16	**N17-C19**	3.93	0.93	0.077
N17-C19	**C9-C11**	3.25	0.38	0.046
N17-C19	**C13-C15**	10.84	0.39	0.083
LP(1)-N20	**N17-C19**	22.94	0.21	0.096
N17-C19	**C9-C11**	23.72	0.09	0.087
N17-C19	**C13-C15**	11.66	0.09	0.064
LP(4)-Cl4	**LP*(6)-Cu(1)**	37.61	0.48	0.176
LP(4)-Cl4	**LP*(8)-Cu(1)**	23.92	0.67	0.160
LP(1)-Cl4	**LP*(8)-Cu(1)**	4.21	6.75	0.074
LP(4)-Cl3	**LP*(6)-Cu(1)**	13.50	0.48	0.106
LP(4)-Cl3	**LP*(7)-Cu(1)**	26.26	0.68	0.171
LP(4)-Cl5	**LP*(6)-Cu(1)**	10.79	0.44	0.092
LP(4)-Cl5	**LP*(7)-Cu(1)**	28.63	0.65	0.175

Table S – 4: Condensed Fukui function fr for $(C_9H_{15}N_3)^+$

	Mulliken atomic charges			***Fukui functions***			
Atoms	N	(N+1)	(N-1)	f^+	f^-	f^0	Δf
1 C	0.407793	-1.661840	0.538042	-2.069633	-0.130249	-1.0998	-1.939
2 C	-0.482102	1.155124	-0.489425	1.637226	0.007323	0.815	1.629
3 C	-0.112434	0.988692	0.025185	1.101126	-0.137919	0.4815	1.239
4 C	-0.000424	-0.285987	0.002690	-0.285563	-0.002693	-0.1445	-0.283
5 C	-0.171389	1.130583	-0.259396	1.301972	0.088007	0.695	1.214
6 H	0.118978	-0.232473	0.152132	-0.3514253	-0.033154	-0.192	-0.318
7 H	0.142146	-1.032656	0.178080	-1.174802	-0.035934	-0.6055	-1.138
8 H	0.124726	-0.365836	0.176657	-0.507982	-0.051931	-0.279	-0.456
9 H	0.158463	-0.145898	0.197601	-0.304361	-0.039438	-0.1715	-0.265
10 N	-0.322383	-0.437578	-0.260069	-0.115195	-0.062314	-0..0875	-0.053
11 N	0.058895	0.106185	0.189098	0.04729	-0.130203	-0.0415	0.177
12 C	-0.313728	0.066287	-0.289230	0.380015	-0.024498	0.178	0.405
13 H	0.134630	0.127443	0.177358	-0.007187	-0.042728	0.025	0.036
14 H	0.101434	-0.042534	0.166661	-0.143968	-0.065227	-0.1045	-0.079
15 C	-0.103640	0.582586	-0.077874	0.686226	-0.025766	0.33	-0.660
16 H	0.108685	-0.017936	0.165159	-0.126621	-0.065474	-0.096	-0.061
17 H	0.100275	-0.132121	0.128167	-0.232396	-0.027892	-0.130	-0.205
18 C	-0.213840	1.533695	-0.148191	1.747535	-0.362031	0.693	2.109
19 H	0.097077	-0.093046	0.120993	-0.190123	-0.023916	-0.107	0.166
20 H	0.117045	-0.637908	0.168833	-0.754953	-0.051788	-0.403	-0.703
21 C	-0.084033	-0.288872	-0.136093	-0.204839	0.05206	-0.076	-0.257
2 H	0.133818	-0.036706	0.187320	-0.170524	-0.053502	-0.879	-0.117
23 H	0.091079	-0.519828	0.122008	-0.610907	-0.030929	-0.821	-0.579
24 N	-0.264193	-0.499932	-0.238865	-0.235739	-0.025328	-0.131	-0.210
25 H	0.173122	-0.259446	0.203161	-0.432568	-0.030039	-0.231	-0.403

Credit Author Statement

Afef Gannouni - She wrote the whole article

Wiem Tahri - She did the biological study

Thierry Roisnel - Single crystal diffraction

Riadh Kefi - He is the Research Supervisor and he gave the plan for this Paper.

I declare that I have no known competing financial interests or personal relationships that could have appeared to influence the work reported in this paper.

Please refer to the *Notes for Authors* of the relevant journal for any special instructions relating to CIF
submission.

PLATON version of 18/05/2022; check.def file version of 17/05/2022

Datablock AG21_02 - ellipsoid plot